



Article

Copper Nanoparticles Synthesized by Chemical Reduction with Medical Applications

Alexandra Pricop¹, Adina Negrea¹ , Bogdan Pascu^{2,*}, Nicoleta Sorina Nemeş^{2,*} , Mihaela Ciopec¹,
Petru Negrea¹, Cătălin Ianăşi³ , Paula Svera⁴ , Delia Muntean⁵ , Alexandra Ivan^{6,7}
and Iustina Mirabela Cristea⁷

- ¹ Faculty of Chemical Engineering, Biotechnologies and Environmental Protection, Politehnica University Timișoara, Victoriei Square, no. 2, 300006 Timișoara, Romania; maria.pricop@student.upt.ro (A.P.); adina.negrea@upt.ro (A.N.); mihaela.ciopec@upt.ro (M.C.); petru.negrea@upt.ro (P.N.)
- ² Research Institute for Renewable Energies—ICER, Politehnica University Timișoara, Gavril Musicescu Street, no. 138, 300774 Timișoara, Romania
- ³ Coriolan Drăgulescu' Institute of Chemistry, Bv. Mihai Viteazul, No. 24, 300223 Timișoara, Romania; ianasic@acad-icht.tm.edu.ro
- ⁴ INCEMC—National Institute for Research and Development in Electrochemistry and Condensed Matter-Timisoara, No. 144 Dr. A. Paunescu Podeanu Street, 300569 Timisoara, Romania; paulasvera@gmail.com
- ⁵ Multidisciplinary Research Centre on Antimicrobial Resistance, Department of Microbiology, University of Medicine and Pharmacy “Victor Babes”, Eftimie Murgu Sq. No. 2, 300041 Timișoara, Romania; muntean.delia@umft.ro
- ⁶ Center of Immuno-Physiology and Biotechnologies (CIFBIOTEH), University of Medicine and Pharmacy “Victor Babes”, Eftimie Murgu Sq. No. 2, 300041 Timișoara, Romania; ivan.alexandra@umft.ro
- ⁷ OncoGen Centre, Clinical County Hospital “Pius Branzeu”, Blvd. Liviu Rebreanu 156, 300723 Timișoara, Romania; mirabela.cristea@oncogen.ro
- * Correspondence: ioan.pascu@upt.ro (B.P.); nicoleta.nemes@upt.ro (N.S.N.)

Abstract: Copper nanoparticles (CuNPs) have attracted attention due to their low cost and high specific surface area. In this work, a simple and inexpensive two-step synthesis method was proposed to prepare highly stable and well-dispersed spherical CuNPs in solution with a particle size of approximately 37 nm. Synthesis of CuNPs was carried on in the presence of complexing agent trisodium citrate (TSC), while for the chemical reduction step, sodium borohydride (NaBH₄) was used. Taking into account the potential of this type of nanoparticles, their synthesis and characterization represent a current and relevant topic in the field. The ability to control the size, shape and properties of CuNPs by adjusting the synthesis parameters (pH, precursor:stabilizer:reductant ratio, homogenization time, temperature) offers extraordinary flexibility in the development of these materials. The combination of characterization techniques such as SEM, EDX, UV–Vis, Raman, FT-IR and AFM provides a thorough understanding of the structure and properties of CuNPs, allowing the modulation of the properties of the obtained nanoparticles in the desired direction. Based on the studies, the copper reduction mechanism was proposed. For the theoretical verification of the size of the experimentally obtained spherical CuNPs, Mie theory was applied. A stability study of the synthesized CuNPs in optimal conditions was performed using UV–Vis analysis at specific time intervals (1, 3, 30 and 60 days), the sample being kept in the dark, inside a drawer at 25 °C. The CuNPs obtained after setting the optimal synthesis parameters (Cu(II):TSC:BH₄[−] = 1:1:0.2, pH = 5, homogenization time 60 min and temperature 25 °C) were then tested to highlight their antibacterial effect on some reference bacterial strains. The obtained CuNPs demonstrated very good antimicrobial efficacy compared to traditional antimicrobials, for both Gram-negative and Gram-positive bacteria. This may reduce the development of antimicrobial resistance, an urgent medical issue. After evaluating the cytotoxic effects of CuNPs on the SKBR3 cancer cell line, a significant decrease in cell proliferation was observed at the 0.5 mg/mL concentration, with



Academic Editor: Maria Carmela Bonaccorsi Di Patti

Received: 6 January 2025

Revised: 8 February 2025

Accepted: 10 February 2025

Published: 14 February 2025

Citation: Pricop, A.; Negrea, A.; Pascu, B.; Nemeş, N.S.; Ciopec, M.; Negrea, P.; Ianăşi, C.; Svera, P.; Muntean, D.; Ivan, A.; et al. Copper Nanoparticles Synthesized by Chemical Reduction with Medical Applications. *Int. J. Mol. Sci.* **2025**, *26*, 1628. <https://doi.org/10.3390/ijms26041628>

Copyright: © 2025 by the authors. Licensee MDPI, Basel, Switzerland. This article is an open access article distributed under the terms and conditions of the Creative Commons Attribution (CC BY) license (<https://creativecommons.org/licenses/by/4.0/>).

a reduction of 89% after 60 h of cultivation. Higher concentrations of CuNPs induced a more rapid cytotoxic effect, leading to an accelerated decline in cell viability.

Keywords: copper nanoparticles; chemical reduction; cytotoxicity effect; antibacterial activity

1. Introduction

Nanotechnology has become a central subject in modern science and industry, transforming fields such as medicine [1,2], electronics [3], energy [4] and environmental science [5] by producing materials with new physical, chemical and biological properties, on a nanometric scale [6,7]. A key component of nanotechnology is the creation of nanostructured materials with sizes ranging from 1 to 100 nm. Depending on the application, nanoparticles can be made of metals, oxides, carbon or polymers. Nanoparticles can be categorized mostly according to their source or precursor, form and material composition [8]. In the last few years, considerable interest has been shown in metal nanoparticles due to their special properties and potential applications in various fields [9,10]. Metallic nanoparticles have special electrical, mechanical, magnetic and chemical capabilities because of their small size and huge specific surface area [11]. These factors have led to the use of metal nanoparticles in a wide range of industries, including electronics, optoelectronics, photonics, biosensors, catalysis and medicine [12–17].

Because of their functional diversity and cost-effectiveness, CuNPs are a significant class of metal nanoparticles that have attracted considerable attention due to their properties [18,19]. Because of their superior electrical conductivity, catalytic qualities and low cost compared to silver and gold material, the synthesis of copper nanoparticles has generated much attention over the years [20–23]. CuNPs can be synthesized using a range of physical, chemical and biological techniques [24,25], each of them with specific advantages and disadvantages. Physically synthesized nanoparticles by methods like mechanical ball milling, physical vapor deposition or gas evaporation have the advantage of uniform distribution and lack solvent contamination, which sets them apart from chemically synthesized ones, such as liquid-phase chemical reduction [26,27], chemical deposition [28] and electrochemical and hydrothermal methods [29,30]. However, they have disadvantages such as slow unfolding over time and high energy consumption at high operating temperature [11,31,32].

Biological methods are increasingly used due to the low cost and non-toxic and environmentally friendly nature of the reducing agents [33,34]. Nanoparticles obtained by biological methods have excellent antimicrobial, anticancer, antidiabetic, anti-inflammatory and antioxidant activities [35]. In terms of chemical methods for obtaining CuNPs, there are a multitude of techniques, including chemical reduction, microwave reduction, sonochemical reduction, electrochemical reduction, photochemical reduction, microemulsion method, hydrothermal method, sol-gel method and thermal decomposition method [33]. Chemical reduction stands out among these techniques due to its selectivity and ability to control the size of the final nanoparticles, two crucial factors for adjusting the biological response of nanoparticles.

Copper sulfate (CuSO_4), copper chloride (CuCl_2) and copper acetate ($\text{Cu}(\text{CH}_3\text{COO})_2$) are some of the most commonly utilized precursors for CuNPs. These precursors are reduced under carefully controlled circumstances to produce the desired nanoparticles [36,37]. For the reduction of Cu(II), the most commonly used reducing agents are sodium borohydride [38], polyols [39,40], hydrazine [41,42], ascorbic acid [43,44], glucose [45,46] and ethylene glycol [45,47], among others.

Therefore, the properties of CuNPs are influenced by the synthesis method used, having a crucial role in their applications, especially in biomedical research. The size of nanoparticles, which can be adjusted during synthesis, is an essential aspect, as it allows for the specific adjustment of optical, catalytic, electrical and biological properties [48].

In these terms, the study's objective is to create CuNPs through chemical reduction with sodium borohydride, applying simple and effective methods for CuNPs synthesis which can be used for different medical applications. For that reason, the material's antibacterial properties and cytotoxic effect were evaluated.

Infections caused by resistant pathogens are a significant cause of severe infections worldwide [49–52]. These pathogens are increasingly difficult to combat due to the resistance acquired over time to the antibiotics used to treat these infections, leading to various forms of cancer in the case of prolonged chronic infections. Therefore, any newly synthesized material that demonstrates antimicrobial properties deserves to be studied in detail, in order to be subsequently used in various medical applications. In this context, it is possible to analyze how CuNPs interact with bacterial strains to combat bacterial proliferation.

On the other hand, the cytotoxic role of certain substances or agents means the ability of these to cause cell death [8,53,54]. This effect can be seen in a variety of situations, including (i) cancer treatment, where a variety of chemotherapies and antimicrobial medications are intended to have a cytotoxic effect on tumor cells, thereby limiting their proliferation; (ii) viral infections, where certain viruses have the ability to cause host cell death as part of their replication cycle, thereby compromising tissue health; and (iii) immune reactions, where specific immune cells, like cytotoxic T lymphocytes, have the function of eliminating diseased or aberrant cells.

The literature reports that CuNPs are more cytotoxic to human cells than other metal oxide nanoparticles [55]. Therefore, CuNPs can be used in the treatment of several types of cancer, including liver cancer [56], lung cancer [57] mammalian cancer [58,59], cervical cancer [60] and pancreatic cancer [61].

It must be noted that copper is an essential trace element vital for human health, serving as a cofactor in processes like blood clotting, hormone maturation and cellular energy production [62–64]. Its redox properties enable participation in critical biochemical reactions, though they can also lead to toxicity [65]. On the other hand, copper plays a significant role in tumor cell death through mechanisms such as cuproptosis, which disrupts mitochondrial respiration, and paraptosis, characterized by endoplasmic reticulum stress and cytoplasmic vacuolization [66]. Copper and its complexes exhibit anticancer effects by inducing oxidative stress, inhibiting angiogenesis, arresting the cell cycle, and regulating energy metabolism [67–69]. Due to their cytotoxic potential against cancer cells, CuNPs have recently become a focus of extensive research [70]. These nanoparticles can generate ROS, causing membrane lipid peroxidation, DNA damage and cell proliferation inhibition, offering innovative strategies for anticancer drug development [71]. Comparative studies on CuNPs and ionic copper cytotoxicity indicate that the toxicity of CuNPs is mainly due to particulate copper rather than released ions [72,73].

In this sense, the obtained CuNPs open the way to antitumor treatments, specific to many types of cancer, and the detailed study of these nanoparticles may allow us to obtain key parameters that are necessary for the manifestation of antitumor action for certain types of cancer cells.

2. Results and Discussion

2.1. Establishing the Optimal Parameters for the Synthesis of CuNPs by Chemical Reduction

2.1.1. Determining the Amount of Complexing Agent in the Synthesis of CuNPs

Determining the optimal amount of complexing agent is an important aspect in many chemical processes, from chemical analysis to materials synthesis. By varying the amount of TSC and keeping the amounts of precursor and reducing agent constant, the following UV–Vis spectra were obtained (Figure 1).

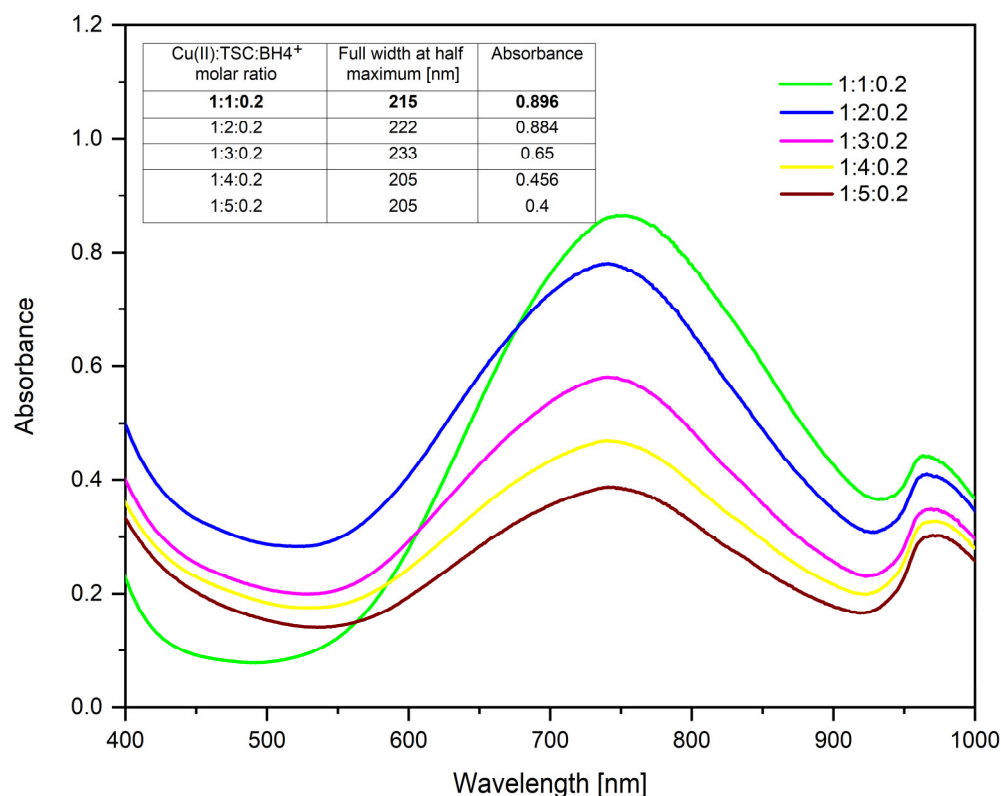


Figure 1. TSC influence (1M CuCl₂ · 2H₂O; 0.2 g NaBH₄; 60 min homogenous time; pH = 5; 25 °C temperature).

According to Figure 1, the surface plasmon resonance existing at wavelength $\lambda = \sim 746$ nm indicates the presence of CuNPs [74]. Using Gaussian fits for the molar ratios Cu(II):TSC:BH₄⁺ used in the synthesis of CuNPs and presented in Figure 2, the full width at half maximum (FWHM) values indicate that the ratios Cu(II):TSC:BH₄⁺ = 1:4:0.2 and Cu(II):TSC:BH₄⁺ = 1:5:0.2 present a lower FWHM value. The absorbance of the material obtained by the synthesis at the molar ratio Cu(II):TSC:BH₄⁺ = 1:1:0.2 is clearly higher, indicating the highest concentration of CuNPs [75]. An increase in the intensity of the surface plasmon resonance band (SPR) indicates the formation and increase in the number of nanoparticles. Furthermore, the SPR band width can be correlated with the nanoparticle size distribution [76]. A wider band indicates a wider size distribution. Based on these considerations, the optimum molar ratio is Cu(II):TSC:BH₄⁺ = 1:1:0.2.

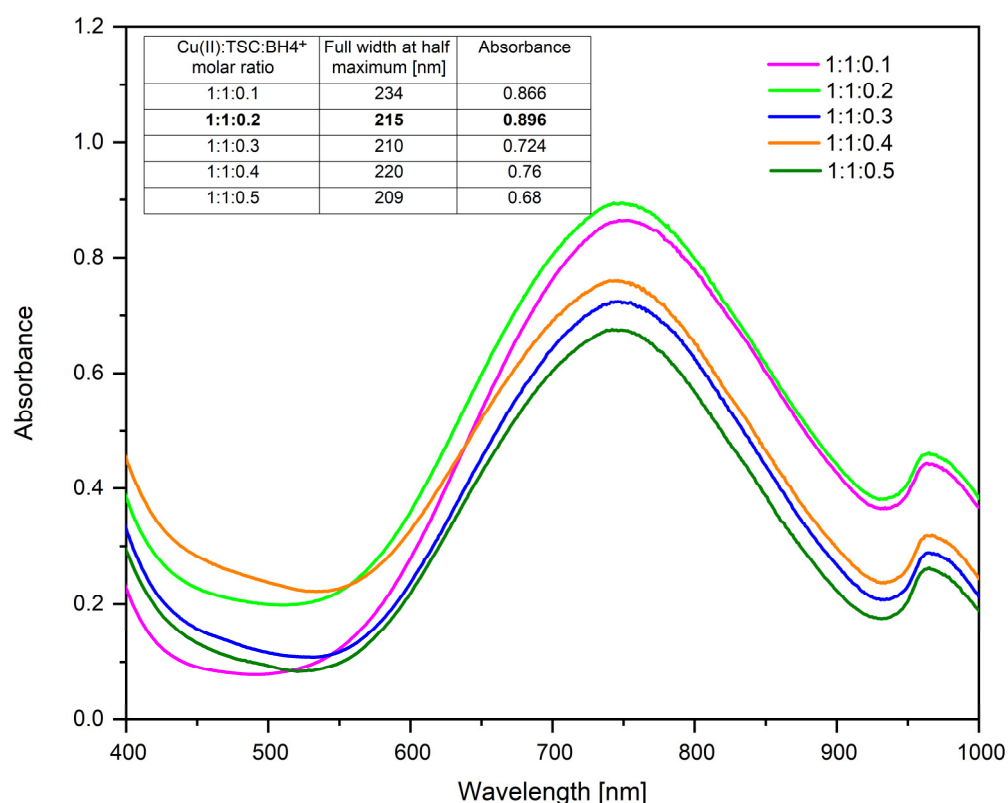


Figure 2. NaBH₄ influence (1M CuCl₂ · 2H₂O; 1M TSC; 60 min homogenous time; pH = 5; 25 °C temperature).

2.1.2. Determining the Amount of Reducing Agent, NaBH₄, in the Synthesis of CuNPs

Chemical reduction with sodium borohydride is one of the most widely used methods, due to the rapid reduction rate and relatively easy control of particle size. Determining the optimal amount of NaBH₄ in the synthesis of CuNPs is a crucial aspect for obtaining nanoparticles with desired sizes, shapes and properties.

The rate at which copper ions are reduced to metallic copper is directly influenced by the concentration of NaBH₄. An excessive amount might cause reduction to occur excessively quickly, which would encourage the creation of large, clumped nanoparticles.

Figure 2 shows the UV–Vis spectra for the molar ratios Cu(II):TSC:NaBH₄⁺, varying the amount of NaBH₄ and keeping the amounts of precursor and complexing agent constant. The FWHM for the studied molar ratios is also established.

From the resulting spectra, it can be observed that at the molar ratio Cu(II):TSC:NaBH₄⁺ = 1:1:0.2 is the highest absorbance, which is correlated with the highest concentration of CuNPs [75]. The full width at half maximum and the absorbance values are also presented in Figure 2.

From the results obtained, it is observed that the values of full width at half maximum are relatively similar, indicating that there are no major differences in terms of the monodispersity of the colloidal system. However, there are differences in terms of absorbance, the optimal one being 0.896, which belongs to the molar ratio Cu(II):TSC:NaBH₄⁺ = 1:1:0.2, which is considered the optimal synthesis ratio.

2.1.3. Establishing the Role of Optimal pH in the Synthesis of CuNPs

pH influences the stability of BH₄[−] and can affect the rate of the precursor's reduction. To highlight the influence of pH, UV–Vis spectra were obtained at different pH values at the molar ratio Cu(II):TSC:NaBH₄⁺ = 1:1:0.2, which was considered the optimal molar ratio (Figure 3).

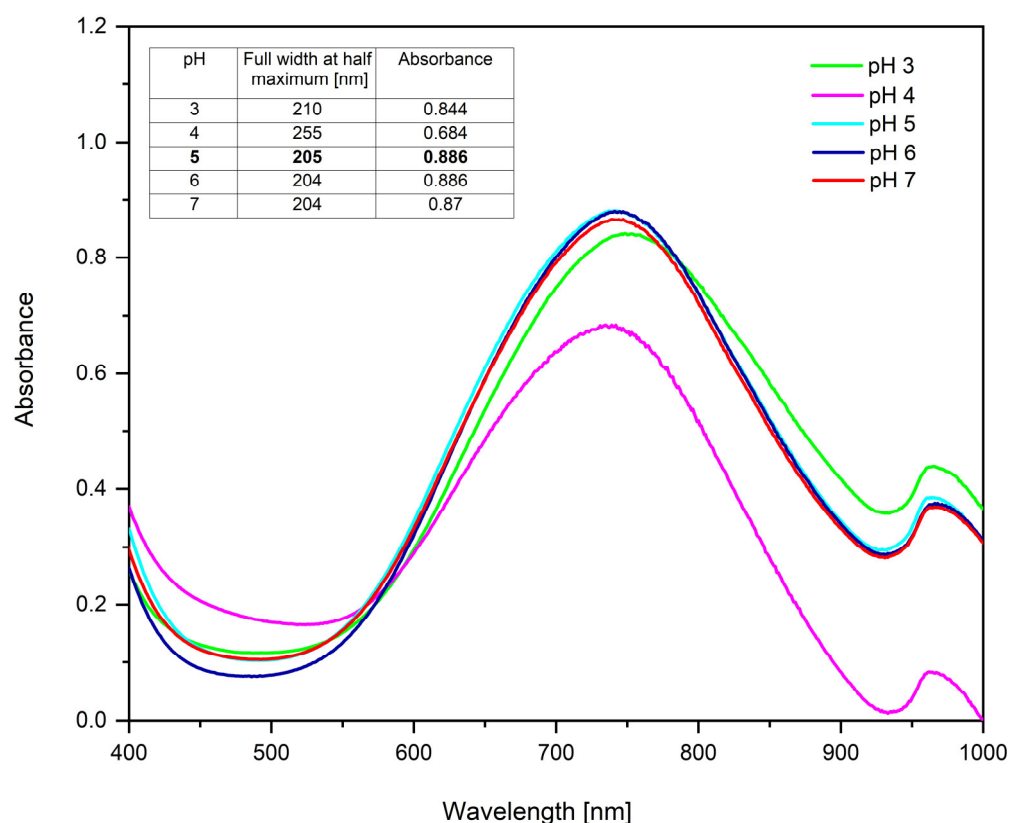


Figure 3. pH influence for optimal molar ratio $\text{Cu(II):TSC:BH}_4^+ = 1:1:0.2$; 60 min homogenous time; 25 °C temperature.

From the spectra obtained, it can be observed that the optimal pH is between 5 and 6, because the spectra's absorbance is higher, indicating the highest concentration of CuNPs [77–79]. Full width at half maximum was also calculated.

From the full width at half maximum analysis, it can be observed that all samples have similar values, indicating that there are no major changes in the monodispersity of the colloidal system. However, at $\text{pH} < 5$ and $\text{pH} > 5$, after 24 h, a precipitate appears, indicating that the nanoparticles are not stable. Therefore, subsequent studies were carried out at $\text{pH} = 5$.

2.1.4. Establishing the Role of Homogenization Time in the Synthesis of CuNPs

Time-dependent UV–Vis measurements provide valuable information about the kinetics of the CuNPs forming and the evolution of their optical properties. Figure 4 shows the UV–Vis spectra for the samples synthesized at different homogenization times, maintaining the molar ratio $\text{Cu(II):TSC:BH}_4^+ = 1:1:0.2$ and $\text{pH} = 5$.

It can be observed that the synthesis does not take place instantly and is completed after 90 min. Moreover, for more detailed study, full width at half maximum determinations were performed. From the obtained results, it is observed that with the increase in the homogenization time, full width at half maximum decreases to $\lambda = 223$ nm, the absorbance increases and implicitly the CuNP concentration increases, which indicates that the monodispersity of the colloidal system increases [80]. As no major changes in absorbance or full width at half maximum occur between 60 and 90 min, a homogenization time of 60 min was considered sufficient for subsequent studies.

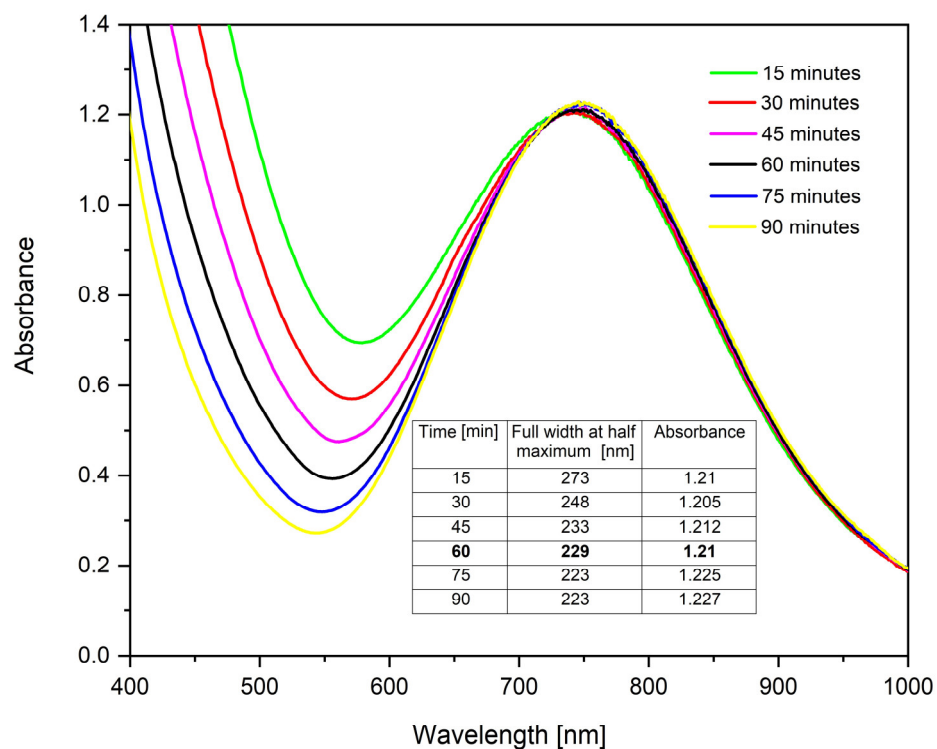


Figure 4. Homogenization time influence for the molar ratio $\text{Cu(II):TSC:BH}_4^+ = 1:1:0.2$; 25 °C temperature and pH = 5.

2.1.5. Establishing the Role of Temperature in the Synthesis of CuNPs

To investigate the influence of temperature on the synthesis of CuNPs, UV-Vis spectra were obtained at different temperature values (Figure 5), maintaining constant the molar ratio $\text{Cu(II):TSC:BH}_4^+ = 1:1:0.2$, pH = 5 and homogenization time of 60 min.

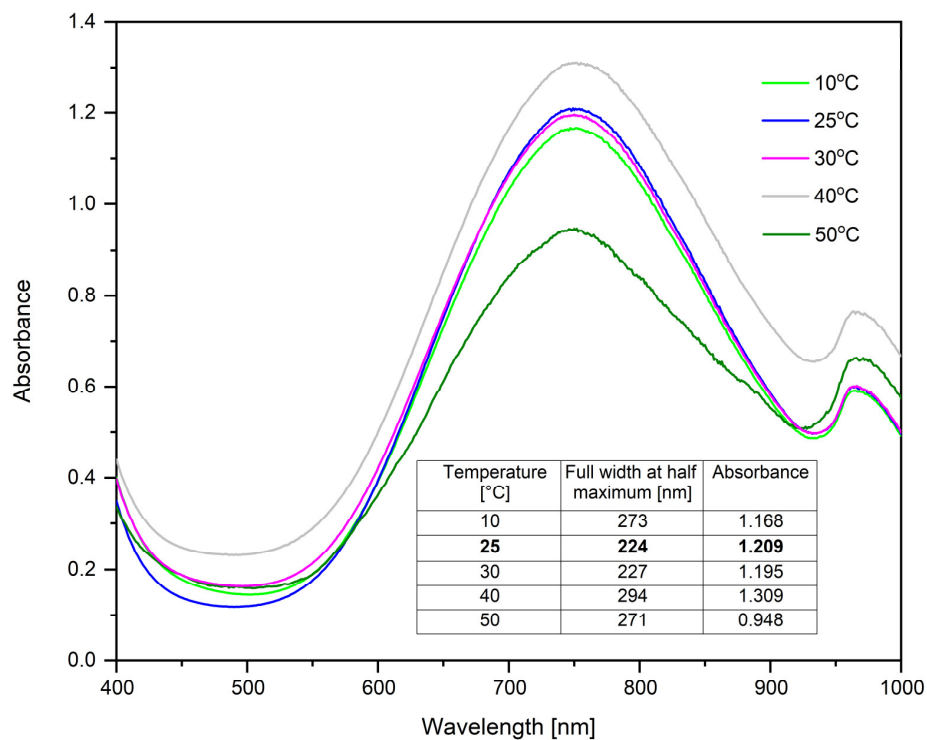


Figure 5. Temperature influence for the molar ratio $\text{Cu(II):TSC:BH}_4^+ = 1:1:0.2$, pH = 5 and homogenization time 60 min.

The optimal temperature for this synthesis is between 10 and 30 °C, as can be seen in Figure 5. Although an increase in absorbance can be observed at 40 °C, this sample is unstable, because after 5 h, a precipitate was observed. The full width at half maximum determination was also performed.

Regarding the sample synthesized at 10 °C, the full width at half maximum is higher compared to the samples synthesized at 25 °C and 30 °C. On the other hand, the absorbance is lower, which indicates that the monodispersity of the colloidal system is better for the samples synthesized at 25 °C and 30 °C. The concentration of CuNPs is higher in the case of the samples synthesized at 25 °C and 30 °C. For economic reasons, the optimal synthesis temperature was considered to be 25 °C.

2.1.6. Study on the Stability of CuNPs over Time

To highlight the stability of CuNPs, UV–Vis spectra were obtained at different time intervals (Figure 6) for the sample synthesized under optimal conditions: molar ratio $\text{Cu(II):TSC:BH}_4^+ = 1:1:0.2$, pH = 5, homogenization time 60 min and temperature 25 °C. Thus, the sample was kept in the dark inside a drawer at 25 °C during this process, resulting in the following spectra:

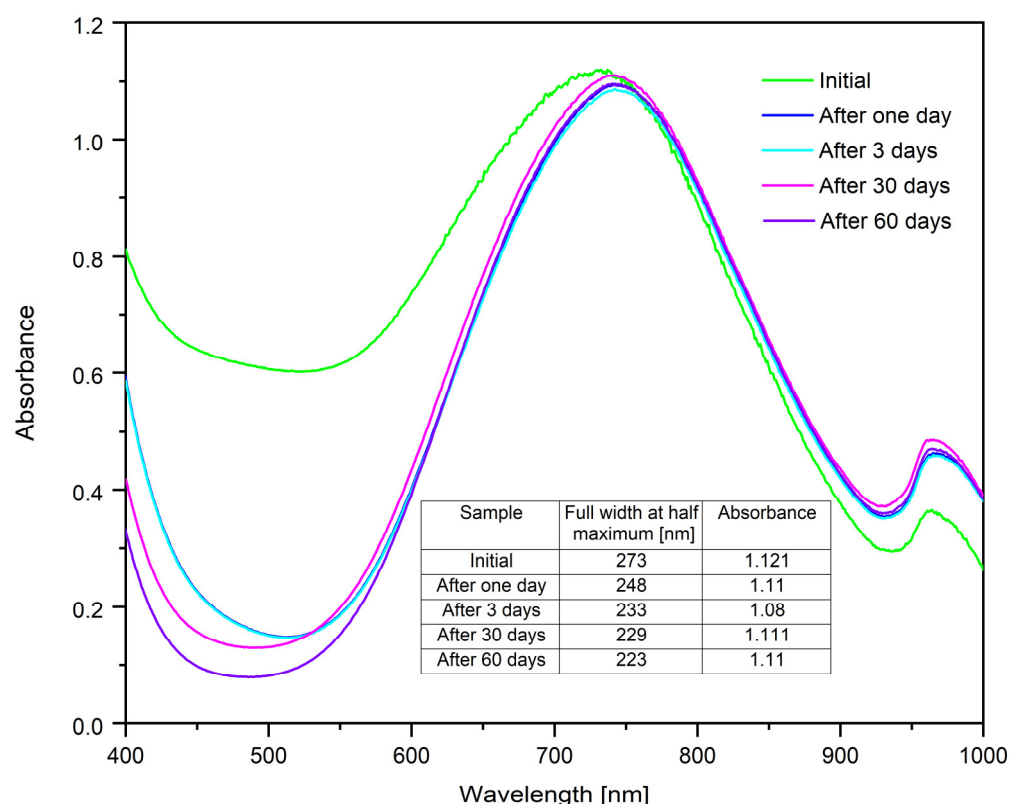
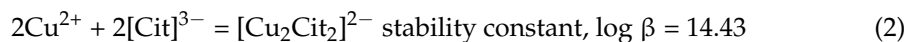


Figure 6. Stability study for the sample synthesized under optimal conditions: molar ratio $\text{Cu(II):TSC:BH}_4^+ = 1:1:0.2$, pH = 5, homogenization time 60 min and temperature 25 °C.

From the resulting spectra, it can be observed that after 24 h there are no major differences in absorbance value. The sample remains stable for 60 days. In order to highlight the monodispersity of the colloidal system, the full width at half maximum values were determined. The acquired results demonstrate that the monodispersity of the CuNPs remains constant, even after a 24 h period. Furthermore, absorbance is steady throughout the investigation.

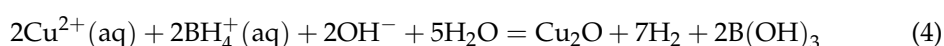
2.1.7. Proposed Mechanism

The citrate ion $[\text{C}_6\text{H}_5\text{O}_7]^{3-}$ complexes Cu^{2+} in a 1:1 molar ratio according to the equations [81]:

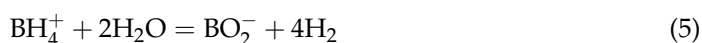


We adopted the stability constants reported by Rode et al. [82], which were mainly based on the work of Daniele et al. [83].

We assume that the mechanism of the reduction process of Cu^{2+} ions is based on the following reactions:



It can be assumed that excess BH_4^+ is hydrolyzed eventually according to the equation [84]:



2.2. Characterization of Synthesized CuNPs

2.2.1. FT-IR Spectroscopy

To highlight the functional groups of the synthesized CuNPs, an FT-IR investigation was performed, as shown in Figure 7.

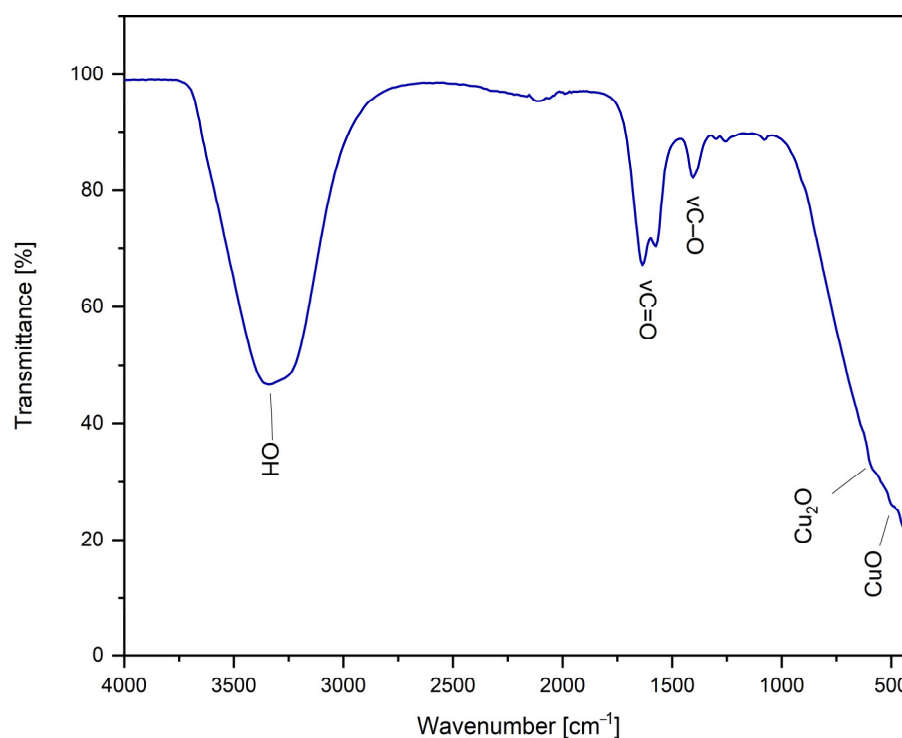


Figure 7. FT-IR spectrum for the sample synthesized under optimal conditions: molar ratio $\text{Cu(II)}:\text{TSC}:\text{BH}_4^+ = 1:1:0.2$, $\text{pH} = 5$, 60 min homogenization time and 25°C temperature.

The broad band present at wave number 3343 cm^{-1} is due to the vibration of the O–H group, specific to water [85]. The bands present at wavenumbers of 1634 cm^{-1} and 1407 cm^{-1} , respectively, are due to the symmetric and asymmetric vibration of the COO^-

group specific to TSC [85,86]. The presence of bands at 487 cm^{-1} and 626 cm^{-1} indicates Cu(II)–O stretching vibrations [87].

2.2.2. Raman Spectroscopy

Raman spectroscopy is a versatile technique for characterizing materials at the molecular level, including nanoparticles. In the case of CuNPs, Raman spectroscopy can provide valuable information about the crystal structure, defects and interactions with the environment.

In Figure 8, the Raman spectrum for CuNPs synthesized under optimal conditions is presented: molar ratio Cu(II):TSC:BH₄⁺ = 1:1:0.2, pH = 5, homogenization time 60 min and temperature 25 °C.

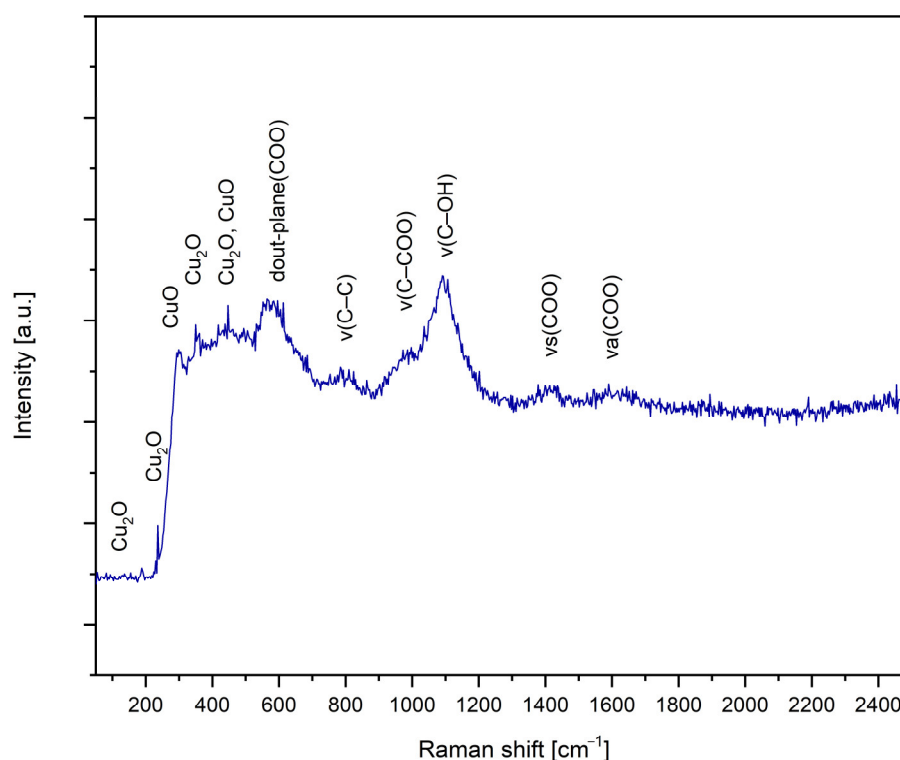


Figure 8. Raman spectrum for the sample synthesized under optimal conditions: molar ratio Cu(II):TSC:BH₄⁺ = 1:1:0.2, pH = 5, 60 min homogenization time and 25 °C temperature.

Raman spectra showed several bands specific to Cu₂O, CuO and Na₃C₆H₅O₇. The observed bands are located at 108 cm⁻¹, 133 cm⁻¹, 235 cm⁻¹, 291 cm⁻¹, 350 cm⁻¹, 454 cm⁻¹, 591 cm⁻¹, 619 cm⁻¹, 811 cm⁻¹, 859 cm⁻¹, 968 cm⁻¹, 1098 cm⁻¹, 1421 cm⁻¹, 1620 cm⁻¹ and 2372 cm⁻¹.

Most of the important bands are observed for Cu₂O at wavelengths 108 cm⁻¹, 133 cm⁻¹, 235 cm⁻¹, 291 cm⁻¹, 454 cm⁻¹ and 591 cm⁻¹ [88,89]. The wavelength shift observed for CuNPs can be attributed to the free π electrons provided by TSC [90]. Both the random distribution on the substrate and the stimulation of the various geometric orientations of the CuNP molecules are responsible for the peak improved performance [91].

The presence of CuO bands at $\sim 350\text{ cm}^{-1}$ and 600 cm^{-1} is observed in a small percentage in the material structure [92].

When it comes to the sodium citrate, the specific bands were identified. The 1421 cm^{-1} wavelength corresponds to the carboxylate symmetric stretching band, $\nu_s(\text{COO})$ [93]. Other specific bands were also identified as follows: 1620 cm^{-1} carboxylate asymmetric stretching

band $\nu_a(\text{COO})$, 1098 cm^{-1} $\nu(\text{C-OH})$, 968 cm^{-1} $\nu(\text{C-COO})$, 859 cm^{-1} $\nu(\text{C-C})$ and 619 cm^{-1} $\delta_{\text{out-plane}}(\text{COO})$ [93].

2.2.3. Scanning Electron Microscopy Analysis (SEM) and Energy-Dispersive X-Ray Spectroscopy (EDX)

To highlight the surface morphology of the synthesized CuNPs, SEM analysis was performed and is presented in Figure 9. To quantify the elemental composition of the synthesized nanoparticles, EDX spectroscopy was performed.

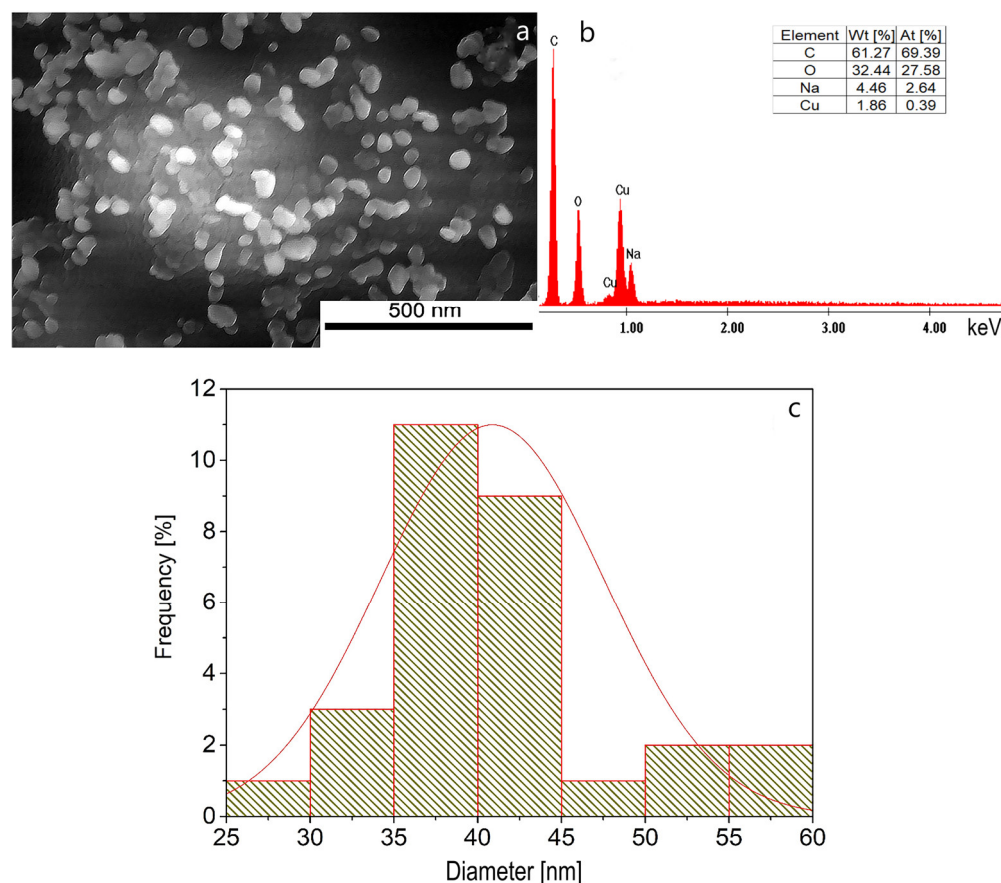


Figure 9. (a) Scanning electron microscopy analysis and (b) energy-dispersive X-ray spectroscopy of the sample synthesized under optimal conditions: molar ratio $\text{Cu(II):TSC:BH}_4^+ = 1:1:0.2$, pH = 5, 60 min homogenization time and $25\text{ }^\circ\text{C}$ temperature, (c) experimental average diameter of CuNPs.

The morphological and topographical properties of CuNPs were examined by scanning electron microscopy. In addition, the SEM study was used to estimate the average size of CuNPs [77,94]. From SEM microscopy (Figure 9a), it is observed that the obtained CuNPs appear in the form of nanoclusters made up of spherical/quasi-spherical nanoparticles, uniformly dispersed. In the EDX spectrum (Figure 9b), the presence of C, O and Na can be observed, all of which are specific to trisodium citrate, and the presence of Cu confirms the formation of copper particles. Carbon and oxygen peaks in the samples verified the presence of carbon-based stabilizers [95]. The C peak in the spectrum can be attributed to the carbon tape used to mount the sample on the stub. From Figure 9c, it can be seen that the average diameter of CuNPs is 37.5 nm.

Starting from the mass percentages given by the EDX analysis and considering that O comes from the citrate ion and copper oxides that are formed after the reduction, we can state that Cu_2O is predominant (78%) and that the rest is CuO (22%). This statement is also supported by the Raman spectrum (Figure 8), where Cu_2O is predominant.

2.2.4. Atomic Force Spectroscopy (AFM)

AFM analysis was performed on a CuNP sample (Figure 10), and roughness data were extracted from the obtained images.

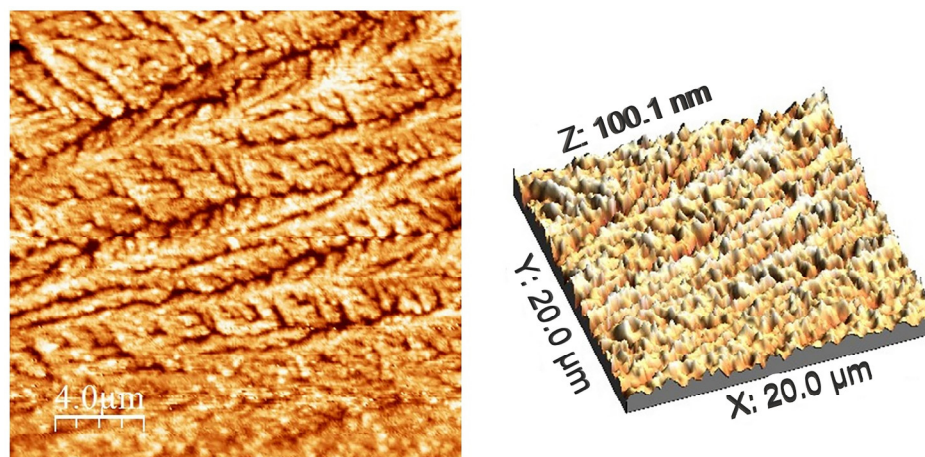


Figure 10. 2D and 3D AFM images of the sample synthesized under optimal conditions: molar ratio Cu(II):TSC:BH₄⁺ = 1:1:0.2, pH = 5, 60 min homogenization time and 25 °C temperature.

Calculated values from AFM images (average roughness (Sa), mean square root roughness (Sq), maximum peak height (Sp), maximum valley depth (Sv), maximum peak-to-valley height (Sy), surface kurtosis (Sku) and surface skewness (Ssk)) are shown in Table 1:

Table 1. Values obtained from AFM analysis.

Sample Name	Ironed Area (μm ²)	Sa (nm)	Sq (nm)	Sp (nm)	Sv (nm)	Sy (nm)	Sku	Ssk
CuNPs	409.886	15.8234	20.0095	46.1396	−53.9583	100.097	2.8463	−0.3843

The material's registered roughness, as determined by the mean square root roughness (Sq) calculation method, is 20.0095 nm, whereas the average roughness (Sa) calculation formula yields 15.8234 nm. The Sp and Sv values refer to the lowest pits and highest peaks on the analyzed sample. Sy is the sum of the Sp and Sv values, which correspond to the sample's highest peaks and lowest pits, respectively. Information on abnormally high peaks or deep valleys is provided by the Ssk and Sku values.

The surface of the acquired CuNP sample is scattered with nanospheres and nano quasi-spheres that resemble the SEM image. The size of the nanoparticles is revealed by the profile analysis of certain regions (Figure 11), which also provides information about the surface features.

However, it should be considered that defects arise during the AFM measurement involving the tip radius curvature effect, resulting in peaks broadening [96]. Therefore, the profile analysis of the spheres is lacking precision, and as result, the calculated size may be erroneous. It is visible that the base of the nanoparticle is always more enlarged in comparison to the tip of the particle. However, the height of the nanoparticles measured in several areas is between 25 and 40 nm, corresponding to the SEM data.

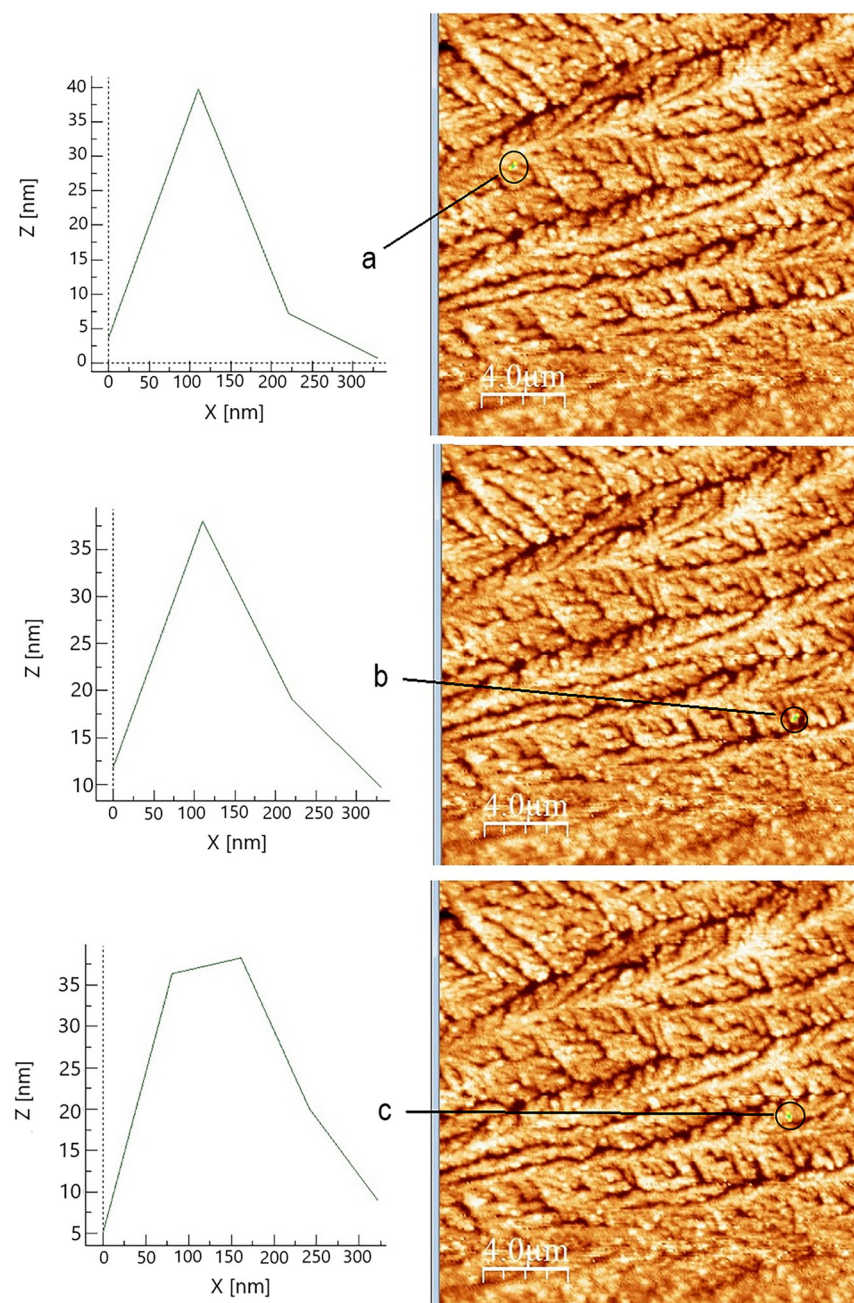


Figure 11. Profile of the selected area of the CuNPs sample synthesized under optimal conditions: molar ratio $\text{Cu(II):TSC:BH}_4^+ = 1:1:0.2$, pH = 5, 60 min homogenization time and 25 °C temperature in three zone: zone (a), zone (b) and zone (c).

2.3. Absorption and Scattering of Electromagnetic Waves by Sphere

To determine the theoretical diameter of CuNPs, a first step involves obtaining a theoretical spectrum “ $C_{\text{ext}}/C_{\text{sca}}/C_{\text{abs}}$ vs. Wavelength”, using the “MiePlot” software for CuNPs. This shows the localized surface plasmon resonance at a wavelength similar to the experimental one, because the localized surface plasmon resonance is strongly influenced by nanoparticle morphology [75]. It is necessary to convert “ C_{ext} ”, obtained from the theoretical spectrum, into the molar absorption coefficient ϵ from the Lambert–Beer law ($A = \epsilon \times l \times C$), using the following relationship:

$$\epsilon = N_A \times C_{\text{ext}} \times \ln 10 \times (10^{-3} \frac{L}{\text{cm}^3}) [\text{L/mol} \times \text{cm}] \quad (6)$$

where N_A = Avogadro's number, i.e., $N_A = 6.022 \cdot 10^{23}$ [L/mol], and C_{ext} = extinction cross section [cm^2].

In order to theoretically estimate the diameter of spherical CuNPs obtained from the synthesis, the sample with optimal synthesis parameters was used, meaning molar ratio $\text{Cu(II)}:\text{TSC}:\text{BH}_4^+ = 1:1:0.2$, $\text{pH} = 5$, homogenization time 60 min and temperature 25°C .

The spectra that are represented in Figure 12 were obtained using the MiePlot software v4.6 [97] and are representative of the synthesized spherical CuNPs particles.

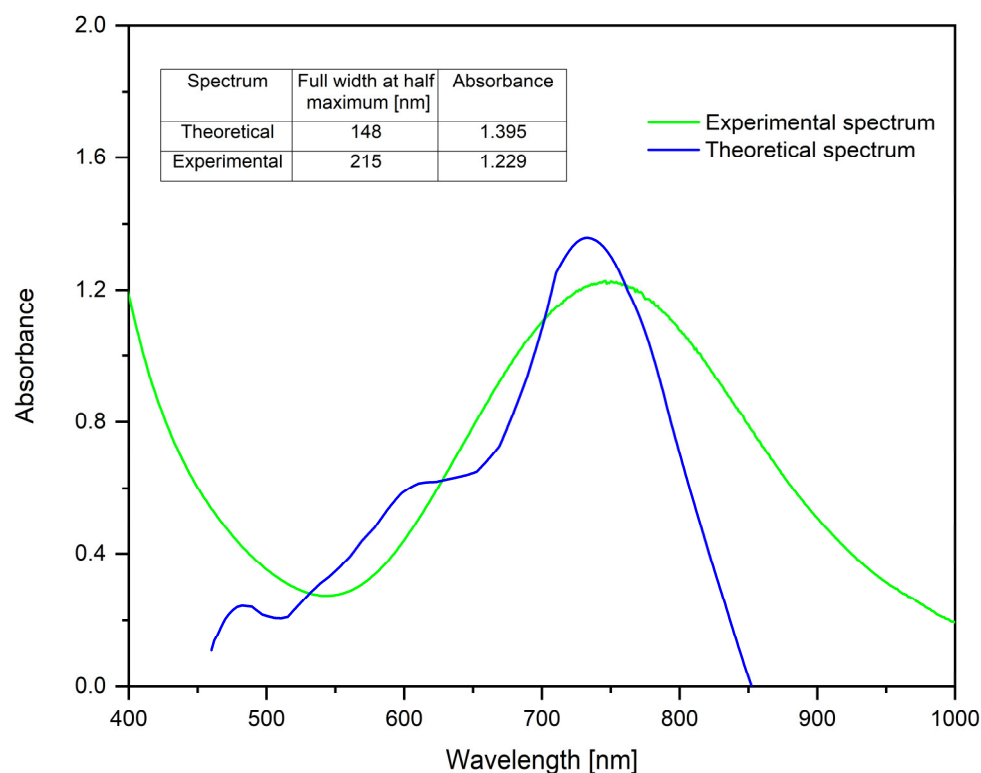


Figure 12. Theoretical determination of CuNP diameter for the sample synthesized under optimal conditions: molar ratio $\text{Cu(II)}:\text{TSC}:\text{BH}_4^+ = 1:1:0.2$, $\text{pH} = 5$, 60 min homogenization time and 25°C temperature.

As can be seen, the theoretical spectrum does not perfectly overlap with the experimental one. This may be because the theoretical spectrum was obtained for theoretical nanoparticles with a diameter of ~ 30 nm, monodisperse. It can also be seen that the full width at half maximum of the experimental spectrum is slightly higher, which implies that the experimentally obtained CuNPs are not exactly monodisperse, the absorbance being lower, so the CuNP concentration is lower compared to the theoretical one.

Based on the calculations, the theoretical size of CuNPs is ~ 30 nm, whereas the size obtained from the SEM micrograph was 37.5 nm. It can be observed that the theoretical result is relatively similar to that determined by SEM analysis, indicating that this theory is useful in the preliminary determination of the size of spherical/quasi-spherical copper nanoparticles.

2.4. CuNP Medical Applications

2.4.1. Microbiologic Tests

The diameter of the inhibitory zone was measured in millimeters to evaluate the antibacterial activity. Following microbiological testing on antibiotic-resistant bacteria, Table 2 displays the determined inhibition diameters on Petri dishes and compares them to the CLSI control test and standards [98].

Table 2. The inhibition diameter for reference strains tested.

ATCC Strains	Tested Compound 10 µL [mm]	Positive Control Test [mm]	Standard CLSI [mm]	Antibiotics Used in Positive Control Test
<i>Streptococcus pneumoniae</i> ATCC 49619	22	30	≥21	ERYTHROMICIN 15 µg
		30	≥23	TETRACICLINE 30 µg
<i>Staphylococcus aureus</i> ATCC 25923	22	29	≥22	CEFOXITIN 30 µg
		26	≥15	GENTAMICIN 10 µg
<i>Escherichia coli</i> ATCC 25922	21	35	≥18	CEFEPIME 30 µg
		24	≥15	GENTAMICIN 10 µg

The values obtained for the diameter disc of inhibition were compared with the interval suggested by the CLSI [98]. The strains used for positive tests are quality control strains, and the interval framing into CLSI measurements demonstrates that the procedure was accurate.

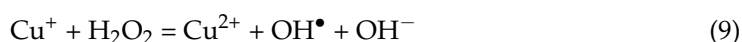
For all strains tested, the inhibition diameter is comparable to that of the CLSI recommendation, which suggests that the tested compound can be associated with an antibiotic in terms of antibacterial activity. At the same time, the tested compound has antibacterial activity against both Gram-negative and Gram-positive strains. This suggests that the tested CuNPs are non-specific and can be used to eliminate a bacterial consortium formed by aerobic bacteria. This is an important aspect in terms of bacterial infections especially, because the predominant aerobic bacteria include *Staphylococcus aureus* and *Escherichia coli* [99], which cause severe infections, and in most cases, patients with malignancy are susceptible to severe infections [100].

The antibacterial activity of CuNPs was compared with that of other metals' nanoparticles. The comparison is presented in Table 3.

Table 3. Antibacterial activity of CuNPs compared with other metallic nanoparticles.

Metallic Nanoparticles Tested	ATCC Strains	Diameter of Inhibition [mm]	References
CuNPs, 10 µL	<i>Streptococcus pneumoniae</i> ATCC 49619	22	Present paper
	<i>Staphylococcus aureus</i> ATCC 25923	22	
	<i>Escherichia coli</i> ATCC 25922	21	
AgNPs, 20 µL	<i>Staphylococcus aureus</i> ATCC 25923	19	[101]
	<i>Pseudomonas aeruginosa</i> ATCC 27853	16	
	<i>Escherichia coli</i> ATCC 25922	16	
	<i>Streptococcus pneumoniae</i> ATCC 49619	11	
	<i>Candida albicans</i> ATCC 90028	20	
AgNPs, 10 µL	<i>Escherichia coli</i> ATCCT 8739	8.9	[102]
	<i>Pseudomonas aeruginosa</i> ATCCT 27853	9.7	
	<i>Staphylococcus aureus</i> ATCC 25923	10.7	
	<i>Salmonella enterica</i> NCTC 160	12.2	
	<i>Bacillus cereus</i> ATCC 14579	10.4	
CuNPs 50 µL	<i>Escherichia coli</i> MTCC 4296	13.00	[103]
	<i>Pseudomonas aeruginosa</i> MTCC 424	16.00	
	<i>Bacillus cereus</i> MTCC 619	12.17	
	<i>Staphylococcus aureus</i> MTCC 316	9.67	

Copper nanoparticles exert an antimicrobial mechanism damaging microbial cells, taking place as a result of reactive oxygen species (ROS) produced through binding or replacing cofactors in metalloproteins [104]. ROS are derivatives which contain unstable oxygen species, such as hydroxyl (OH^\bullet), hydrogen peroxide (H_2O_2) and superoxide ($\text{O}_2^{\bullet-}$) [105]. Copper can generate ROS through reactions such as [106]:



Copper accepts and donates an electron, jumping between Cu^+ and Cu^{2+} oxidation states, producing $\text{O}_2^{\bullet-}$ and the hydroxyl OH^\bullet group. These are highly reactive species which lead to lipid peroxidation, protein oxidation and thus DNA damage [107,108].

The fact that CuNPs obtained by the method presented in this study have good antibacterial activity toward both Gram-positive strains tested is a key for its use against infections with Gram-positive strains, because in recent decades, the incidence of infections with Gram-positive bacteria has increased [109].

2.4.2. Cytotoxicity Tests

A dose-dependent response was observed following exposure to CuNPs synthesized under optimal conditions—namely, molar ratio $\text{Cu(II):TSC:BH}_4^+ = 1:1:0.2$, pH = 5, homogenization time 60 min and temperature 25 °C—by the SKBR3 cancer cell line. At a concentration of 0.05% (0.5 mg/mL), no significant cytotoxic effects were observed on SKBR3 cells during the initial 60 h, when the cells entered a plateau phase followed by a period of significant decrease in proliferation (Figure 13). However, significant cytotoxicity was evident at concentrations ranging from 0.1% (1 mg/mL) to 0.2% (2 mg/mL) compared to untreated cells ($p < 0.001$), indicating a substantial reduction in cell viability.

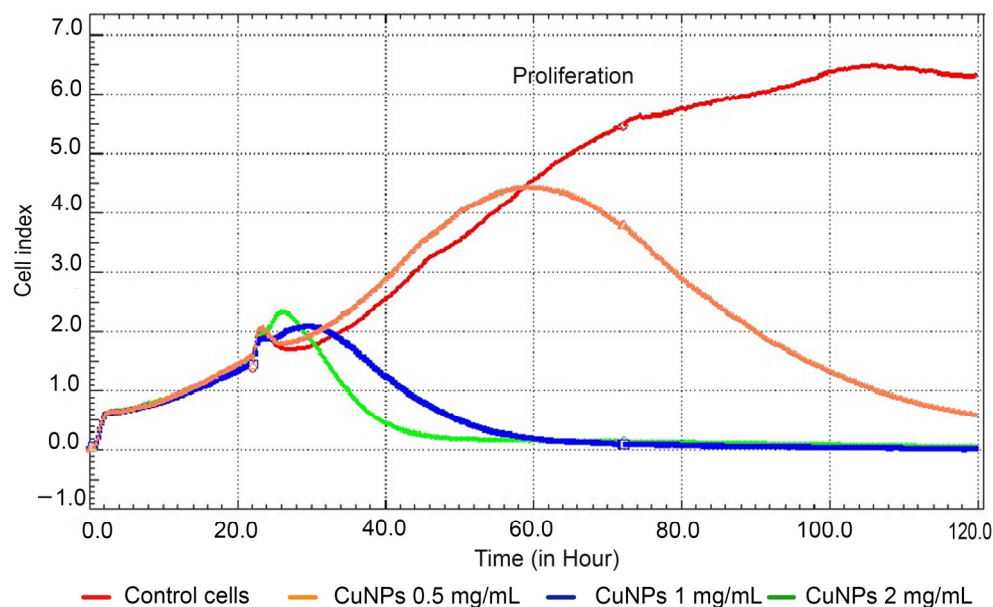


Figure 13. Cytotoxic effects of CuNPs on SKBR3 cells using the xCELLigence system.

The cell index curve illustrates the initial phase of cell adhesion and spreading, followed by a gradual proliferation phase for untreated cells (in red). In contrast, cells treated with CuNPs exhibit a dose-dependent decrease in proliferation ($p < 0.001$). Data are presented as the mean cell index value \pm SD.

The study highlights the dose-dependent cytotoxic effects of CuNPs on SKBR3 cancer cells. At low concentrations (0.5 mg/mL), the CuNPs showed minimal impact on cell viability within the first 60 h. However, higher concentrations (1–2 mg/mL) induced pronounced cytotoxicity, indicating their potential as therapeutic agents for cancer treatment. Similar findings were reported by Abdollahzadeh et al., who observed comparable effects in other breast and colorectal cancer cell lines, including MCF-7 and HCT-116 [110].

3. Materials and Methods

3.1. Synthesis Method

The synthesis of CuNPs is a continuously developing field, and precise control of their size, shape and properties is essential for optimizing the performance of the obtained materials, with specific applications.

To establish the optimal conditions for the synthesis of CuNPs, specific synthesis parameters were established, namely the precursor:reducing agent:complexing agent ratio, the pH of the reaction mass, the homogenizing time and the temperature.

The copper precursor used in this study was copper chloride (Carl Roth, Karlsruhe, Germany), $\text{CuCl}_2 \cdot 2\text{H}_2\text{O}$ 1M. The reducing agent used was sodium borohydride, NaBH_4 (Merck, Darmstadt, Germany). The complexing agent was trisodium citrate, TSC (Chimexim, Bucharest, Romania), $\text{Na}_3\text{C}_6\text{H}_5\text{O}_7 \cdot 3\text{H}_2\text{O}$ 1 M.

First, 1M TSC was stirred with 1M $\text{CuCl}_2 \cdot 2\text{H}_2\text{O}$ for 10 min to homogenize. Then, NaBH_4 was added to the reaction mixture, followed by homogenization for different time periods (5, 30, 45, 60, 75 and 90 min). The synthesis is schematically presented in Figure 14.

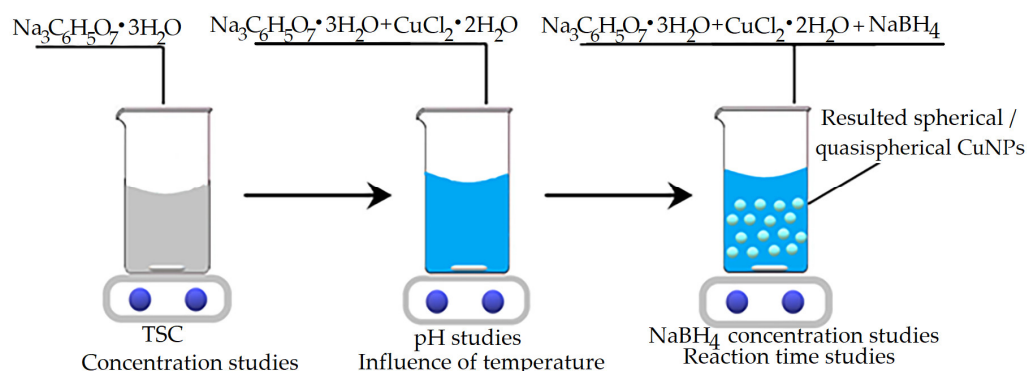


Figure 14. Schematic depiction of CuNP synthesis.

To determine the optimal amount of complexing agent, TSC, the amount was varied so that the molar ratios ($\text{Cu(II)}:\text{TSC}:\text{BH}_4^+$) would be 1:1:0.2; 1:2:0.2; 1:3:0.2; 1:4:0.2 and 1:5:0.2.

To determine the optimal amount of reducing agent, NaBH_4 , the amounts of precursor and complexing agent were kept constant, varying the amount of reducing agent so as to obtain the molar ratios $\text{Cu(II)}:\text{TSC}:\text{BH}_4^+ = 1:1:0.1; 1:1:0.2; 1:1:0.3; 1:1:0.4; 1:1:0.5$.

To establish the optimal pH, the pH of the reaction mass was adjusted with a NaOH solution in the range of pH 3–7 using a Mettler Toledo pH meter (Mettler-Toledo International Inc., Columbus, OH, USA). The chosen $\text{Cu(II)}:\text{TSC}:\text{BH}_4^+$ ratio was the optimal ratio established previously.

The optimum temperature was established by varying the temperature in the range of 10–50 °C by cooling with ice or heating. The reaction mass was set to the optimum $\text{Cu(II)}:\text{TSC}:\text{BH}_4^+$ ratio.

The stability study of the synthesized CuNPs was performed by UV–Vis analysis at different time intervals (1, 3, 30 and 60 days). During the tests, the samples were kept in the dark, at a temperature of 25 °C.

The produced nanoparticles were evaluated using physicochemical techniques including UV–Vis spectroscopy (Varian Cary 50, Varian Inc., Santa Clara, CA, USA), Raman spectroscopy (at room temperature and 514 nm laser excitation with Shamrock 500i Spectrograph, Angor, UK), FT-IR spectroscopy (Bruker Platinum ATR-QL Diamond spectrometer, Billerica, MA, USA), scanning electron microscopy (SEM) and energy-dispersive X-ray spectroscopy (EDX) (Quanta FEG 250 Scanning, FEI Company, Hillsbro, OR, USA) and atomic force microscopy (AFM) (room-temperature scanning probe microscopy platforms system, with a resonance of 30–40 kHz and a chromium-doped tip with a radius of 20 nm, MultiView-2000, Nanonics Imaging Ltd., Jerusalem, Israel) in order to gain a better knowledge of the structure and characteristics of CuNPs.

In physical optics, the scattering of light by spherical particles is described mathematically by Mie theory. In this study, Mie theory was used to theoretically assess the size of spherical CuNPs. Because it makes it possible to calculate the interaction between light and particles of sizes similar to the incident light's wavelength, this theory is crucial for characterizing nanoparticles. The MiePlot v4.6 software includes a database which is used to carry out the required computations for the produced copper nanospheres.

3.2. Microbiological Tests

3.2.1. Inoculum Preparation

A sterile cotton swab was used to pick colonies from a 24 h culture on Columbia agar + 5% sheep blood (Oxoid, Germany). The picked colonies were transferred to 0.9% saline, and an inoculum was obtained. The inoculum density was adjusted to 0.5 McFarland ($1\text{--}2 \times 10^8$ microorganisms/mL) by addition of bacterial colonies or saline solution. The standardized inoculum was used within 15 min of preparation.

3.2.2. Inoculation of Agar Plates

A sterile cotton swab was used to take the inoculum from the 0.5-McFarland-density suspension of the following bacterial strains: Gram-negative *Escherichia coli* ATCC 25922, and Gram-positive *Staphylococcus aureus* ATCC 29213 and *Streptococcus pneumoniae* ATCC 49619 (Microbiologics, Couëron, France). Mueller–Hinton agar (Oxoid, Germany) was inoculated with 0.1 mL of this standardized suspension, which was distributed uniformly over the entire surface of the agar. To test the antibacterial effect on *Streptococcus pneumoniae*, Mueller–Hinton medium supplemented with sheep blood (Oxoid, Germany) was used.

Of the compound to be tested, 10 µL was added to each empty disc (BioMaxima, Lublin, Poland), which, after impregnation, was dried in a sterile environment. Each disc with the test material was subsequently placed in the center, on the surface of the medium, for each microbial strain tested, while other antibiotic microtablets were placed around it and used as controls for the interpretation of the antibacterial effect.

3.2.3. Application of Antimicrobial Discs

Positive controls used for testing were represented by 2 antibiotics for each strain tested (Oxoid, Germany). For the *E. coli* strain, 10 µg gentamicin and 30 µg cefepime were used; for *S. aureus* testing, 30 µg cefoxitin and 10 µg gentamicin were used; and for *S. pneumoniae*, 15 µg erythromycin and 30 µg tetracycline were used.

A disc impregnated with 10 µL of the test compound was also applied, to test the sensitivity to this compound.

3.2.4. Principle of the Diffusimetric Method

The plates inoculated with the microbial suspensions were incubated at 35 ± 2 °C for 24 h.

The presence of sensitivity to the antibiotics used was considered a positive control.

The diameters of the inhibition zones obtained (which include the diameter of the disc) were measured in mm using a ruler. The reading of the inhibition zone limit was assessed with the naked eye, with the plate held approximately 30 cm from the eye.

3.3. Biological Test

Cell Culture and Treatment

The cells were maintained in McCoy's 5A medium (Gibco, Life Technologies, Grand Island, NY, USA) containing 10% FBS (PromoCell, Heidelberg, Germany) and 1% penicillin–streptomycin (Gibco, Life Technologies, Grand Island, NY, USA) in a CO₂ incubator at 37 °C. Cell toxicity of CuNPs was assessed on the human breast cancer cell line SKBR3 (catalog number HTB-30, American Type Culture Collection, Virginia, USA) using the xCELLigence system (ACEA Biosciences, San Diego, CA, USA). This system enables real-time, non-invasive monitoring of adherent cell proliferation and viability through electronic impedance measurement. For these measurements, cells were seeded in 200 µL of culture medium in specialized microplates (E-Plate, ACEA Biosciences, San Diego, CA, USA) at nanoparticle concentrations of 0.05% (0.5 mg/mL), 0.1% (1 mg/mL) and 0.2% (2 mg/mL). The system continuously monitored cell attachment, spreading and proliferation. Twenty-four hours after seeding, nanoparticle treatments were applied, and cell behavior was tracked for up to 120 h. Cell impedance was expressed as the cell index, a parameter automatically calculated by the system's software (xCelligence, RTCA Software 1.2, version 1.2.1). The cell index is a relative measurement, a unitless parameter that is automatically determined by dividing the change in electrical impedance (R) at a specific frequency by the nominal impedance value [111]. This method provided precise and dynamic insights into cell responses to CuNPs.

The percentage of cytotoxicity (%) in cells exposed to CuNPs at different concentrations was calculated relative to the control values based on the cell index [112], following the formula:

$$\text{Cytotoxicity}(\%) = \left(1 - \frac{\text{cell index of treated group at time } t}{\text{cell index of control group at time } t}\right) \times 100 \quad (10)$$

The results are presented as mean value ± standard deviation. A one-way ANOVA test was used to determine the statistical difference between the experimental groups.

4. Conclusions

The present study illustrates a simple, convenient and significant method for the synthesis of CuNPs.

The study demonstrated the possibility of synthesizing CuNPs by chemical reduction using NaBH₄ as a reducing agent and TSC as a complexing agent. The established optimal synthesis conditions are: molar ratio Cu(II):TSC:BH₄⁺ = 1:1:0.2, pH = 5, homogenization time 60 min and temperature 25 °C. The synthesized CuNPs were characterized by physicochemical characterization using UV–Vis spectroscopy. At λ = ~746 nm, the presence of CuNPs was revealed. SEM micrographs and EDX spectra indicated that the synthesized CuNPs are spherical/quasi-spherical in shape, with a diameter of ~37 nm. The particle size was also confirmed by AFM investigation.

FT-IR spectroscopy highlighted the presence of vibrational bands for Cu–O. Using Raman spectroscopy, the presence of a mixture of Cu₂O and CuO particles was identified. The sample remained stable for 60 days. In order to highlight the monodispersity of the colloidal system, it was determined that the theoretical diameter of CuNPs involves obtaining a theoretical spectrum “C_{ext}/C_{sca}/C_{abs} vs. Wavelength”, using the “MiePlot” software v4.6 for CuNPs, which was compared with the experimentally obtained spectrum. Based

on the calculations, the theoretical size of CuNPs was ~30 nm, whereas the size obtained from the SEM micrograph was 37.5 nm. Thus, we can conclude that the theoretical result is relatively similar to that determined by SEM analysis, indicating that Mie theory is useful in the determination of the size of spherical/quasi-spherical nanoparticles, in general.

CuNPs reveal very good antibacterial activity, on both Gram-negative and Gram-positive bacteria. Their antibacterial activity is comparable to the CLSI standard recommendation for all the tested strains. This suggests that CuNPs can be further investigated for medical application in terms of bacterial infection eradication.

The capacity of metallic nanoparticles to overcome antibiotic resistance has been attributed to their special physicochemical characteristics, which allow for the exploitation of several new bactericidal routes in order to provide antimicrobial activity. Metallic nanoparticles have a wide range of activity because of the typically non-specific binding between metal ions and the biomolecules of microorganisms.

This study suggests that CuNPs exhibit dose-dependent cytotoxicity on the SKBR3 cancer cell line. However, the increase in cytotoxic effect requires further investigation, particularly with normal cell lines, to assess the potential of CuNPs as therapeutic agents for cancer treatment. Additional research is essential to elucidate the underlying mechanisms driving cytotoxicity and optimize these CuNPs for their use in therapeutic applications.

Author Contributions: Conceptualization, A.N. and N.S.N.; formal analysis, A.P., B.P., I.M.C., C.I., P.S. and A.I.; investigation, A.P., B.P., N.S.N., P.S., D.M. and A.I.; methodology, A.N., P.N., D.M., A.I. and I.M.C.; software, B.P. and C.I.; validation, A.N., I.M.C., P.N., D.M. and M.C.; writing—original draft, A.P., A.N. and N.S.N.; writing—review and editing, A.N., N.S.N. and C.I. All authors have read and agreed to the published version of the manuscript.

Funding: This research received no external funding.

Institutional Review Board Statement: Not applicable.

Informed Consent Statement: Not applicable.

Data Availability Statement: Data are contained within the article.

Conflicts of Interest: The authors declare no conflicts of interest.

References

1. Saini, R.; Saini, S.; Sharma, S. Nanotechnology: The future medicine. *J. Cutan. Aesthetic Surg.* **2010**, *3*, 32–33. [\[CrossRef\]](#) [\[PubMed\]](#)
2. Ramos, A.P.; Cruz, M.A.E.; Tovani, C.B.; Ciancaglini, P. Biomedical applications of nanotechnology. *Biophys. Rev.* **2017**, *9*, 79–89. [\[CrossRef\]](#)
3. Payal; Pandey, P. Role of Nanotechnology in Electronics: A Review of Recent Developments and Patents. *Recent Pat. Nanotechnol.* **2022**, *16*, 45–66. [\[CrossRef\]](#) [\[PubMed\]](#)
4. Malik, S.; Muhammad, K.; Waheed, Y. Nanotechnology: A Revolution in Modern Industry. *Molecules* **2023**, *28*, 661. [\[CrossRef\]](#) [\[PubMed\]](#)
5. Guerra, F.D.; Attia, M.F.; Whitehead, D.C.; Alexis, F. Nanotechnology for Environmental Remediation: Materials and Applications. *Molecules* **2018**, *23*, 1760. [\[CrossRef\]](#) [\[PubMed\]](#)
6. Haleem, A.; Javaid, M.; Singh, R.P.; Rab, S.; Suman, R. Applications of nanotechnology in medical field: A brief review. *Glob. Health J.* **2023**, *7*, 70–77. [\[CrossRef\]](#)
7. Bayda, S.; Adeel, M.; Tuccinardi, T.; Cordani, M.; Rizzolio, F. The history of nanoscience and nanotechnology: From chemical–physical applications to nanomedicine. *Molecules* **2019**, *25*, 112. [\[CrossRef\]](#)
8. Harishchandra, B.D.; Pappuswamy, M.; Antony, P.U.; Shama, G.; Pragatheesh, A.; Arumugam, V.A.; Periyaswamy, T.; Sundaram, R. Copper Nanoparticles: A Review on Synthesis, Characterization and Applications. *Asian Pac. J. Cancer Biol.* **2020**, *5*, 201–210. [\[CrossRef\]](#)
9. Burlec, A.F.; Corciova, A.; Boev, M.; Batir-Marin, D.; Mircea, C.; Cioanca, O.; Danila, G.; Danila, M.; Bucur, A.F.; Hancianu, M. Current Overview of Metal Nanoparticles' Synthesis, Characterization, and Biomedical Applications, with a Focus on Silver and Gold Nanoparticles. *Pharmaceuticals* **2023**, *16*, 1410. [\[CrossRef\]](#)

10. Lu, R.; Hao, W.; Kong, L.; Zhao, K.; Bai, H.; Liu, Z. A simple method for the synthesis of copper nanoparticles from metastable intermediates. *RSC Adv.* **2023**, *13*, 14361–14369. [[CrossRef](#)]
11. Parveen, F.; Sannakki, B.; Mandke, M.; Pathan, H. Copper nanoparticles: Synthesis methods and its light harvesting performance. *Sol. Energy Mater. Sol. Cells* **2016**, *144*, 371–382. [[CrossRef](#)]
12. Daniel, M.C.; Astruc, D. Gold nanoparticles: Assembly, supramolecular chemistry, quantum-size-related properties, and applications toward biology, catalysis, and nanotechnology. *Chem. Rev.* **2004**, *104*, 293–346. [[CrossRef](#)] [[PubMed](#)]
13. Tian, Y.; Tatsuma, T. Plasmon-induced photoelectrochemistry at metal nanoparticles supported on nanoporous TiO₂. *Chem. Commun.* **2004**, *16*, 1810–1811. [[CrossRef](#)] [[PubMed](#)]
14. Kalidindi, S.B.; Sanyal, U.; Jagirdar, B.R. Nanostructured Cu and Cu@Cu₂O core shell catalysts for hydrogen generation from ammonia–borane. *Phys. Chem. Chem. Phys.* **2008**, *10*, 5870–5874. [[CrossRef](#)]
15. Grzelczak, M.; Pérez-Juste, J.; Mulvaney, P.; Liz-Marzán, L.M. Shape control in gold nanoparticle synthesis. *Chem. Soc. Rev.* **2008**, *37*, 1783–1791. [[CrossRef](#)]
16. Shahsavari, S.; Hadian-Ghazvini, S.; Saboor, F.H.; Oskouie, I.M.; Hasany, M.; Simchi, A.; Rogach, A.L. Ligand functionalized copper nanoclusters for versatile applications in catalysis, sensing, bioimaging, and optoelectronics. *Mater. Chem. Front.* **2019**, *3*, 2326–2356. [[CrossRef](#)]
17. Molahalli, V.; Sharma, A.; Bijapur, K.; Soman, G.; Shetty, A.; Sirichandana, B.; Patel, B.G.M.; Chattham, N.; Hegde, G. Properties, Synthesis, and Characterization of Cu-Based Nanomaterials. In *Copper-Based Nanomaterials in Organic Transformations*; Srivastava, A., Srivastava, A., Eds.; American Chemical Society: Washington, DC, USA, 2024; Volume 1466, pp. 1–33.
18. Wang, P.; Meng, S.; Zhang, B.; He, M.; Li, P.; Yang, C.; Li, G.; Li, Z. Sub-1 nm Cu₂O Nanosheets for the Electrochemical CO₂ Reduction and Valence State–Activity Relationship. *J. Am. Chem. Soc.* **2023**, *145*, 26133–26143. [[CrossRef](#)]
19. Xu, Z.; Wang, W.; Xu, Y.; Song, S.; Yu, J.; Song, W.; Xu, H.; Fu, H.; Li, Z. Visible Light-Promoted Goldberg Reaction Driven by a Preponderant Facet of CuO Nanocrystals. *ACS Catal.* **2023**, *13*, 13920–13930. [[CrossRef](#)]
20. Sui, Y.; Fu, W.; Yang, H.; Zeng, Y.; Zhang, Y.; Zhao, Q.; Li, Y.; Zhou, X.; Leng, Y.; Li, M.; et al. Low Temperature Synthesis of Cu₂O Crystals: Shape Evolution and Growth Mechanism. *Cryst. Growth Des.* **2010**, *10*, 99–108. [[CrossRef](#)]
21. Xu, J.; Yu, K.; Zhu, Z. Synthesis and field emission properties of Cu dendritic nanostructures. *Phys. E Low-Dimens. Syst. Nanostructures* **2010**, *42*, 1451–1455. [[CrossRef](#)]
22. Chang, Y.; Lye, M.L.; Zeng, H.C. Large-scale synthesis of high-quality ultralong copper nanowires. *Langmuir* **2005**, *21*, 3746–3748. [[CrossRef](#)] [[PubMed](#)]
23. Fritea, L.; Banica, F.; Costea, T.O.; Moldovan, L.; Dobjanschi, L.; Muresan, M.; Cavalu, S. Metal Nanoparticles and Carbon-Based Nanomaterials for Improved Performances of Electrochemical (Bio)Sensors with Biomedical Applications. *Materials* **2021**, *14*, 6319–6355. [[CrossRef](#)] [[PubMed](#)]
24. Nam, N.H.; Luong, N.H. Chapter 7—Nanoparticles: Synthesis and applications. In *Materials for Biomedical Engineering*; Grumezescu, V., Grumezescu, A.M., Eds.; Elsevier: Amsterdam, The Netherlands, 2019; pp. 211–240. [[CrossRef](#)]
25. Crisan, M.C.; Mocan, T.; Mocan, L. Copper Nanoparticles: Synthesis and Characterization, Physiology, Toxicity and Antimicrobial Applications. *Appl. Sci.* **2022**, *12*, 141. [[CrossRef](#)]
26. Tan, K.S.; Cheong, K.Y. Advances of Ag, Cu, and Ag–Cu alloy nanoparticles synthesized via chemical reduction route. *J. Nanoparticle Res.* **2013**, *15*, 1537. [[CrossRef](#)]
27. Pike, S.D.; White, E.R.; Regoutz, A.; Sammy, N.; Payne, D.J.; Williams, C.K.; Shaffer, M.S.P. Reversible Redox Cycling of Well-Defined, Ultrasmall Cu/Cu₂O Nanoparticles. *ACS Nano* **2017**, *11*, 2714–2723. [[CrossRef](#)]
28. Liu, Z.; Bando, Y. A Novel Method for Preparing Copper Nanorods and Nanowires. *Adv. Mater.* **2003**, *15*, 303–305. [[CrossRef](#)]
29. Gan, Y.; Jayatissa, A.; Yu, Z.; Chen, X.; Li, M. Hydrothermal Synthesis of Nanomaterials. *J. Nanomater.* **2020**, *2020*, 8917013. [[CrossRef](#)]
30. Darr, J.A.; Zhang, J.; Makwana, N.M.; Weng, X. Continuous Hydrothermal Synthesis of Inorganic Nanoparticles: Applications and Future Directions. *Chem. Rev.* **2017**, *117*, 11125–11238. [[CrossRef](#)]
31. Iravani, S.; Korbekandi, H.; Mirmohammadi, S.V.; Zolfaghari, B. Synthesis of silver nanoparticles: Chemical, physical and biological methods. *Res. Pharm. Sci.* **2014**, *9*, 385–406.
32. Roy, N.K.; Foong, C.S.; Cullinan, M.A. Effect of size, morphology, and synthesis method on the thermal and sintering properties of copper nanoparticles for use in microscale additive manufacturing processes. *Addit. Manuf.* **2018**, *21*, 17–29. [[CrossRef](#)]
33. Tito, I.A.; Uddin, S.; Islam, S.; Bhowmik, S. Copper Nanoparticle (CuNP's) Synthesis: A review of the various ways with Photocatalytic and Antibacterial Activity. *Orient. J. Chem.* **2021**, *37*, 1030–1040. [[CrossRef](#)]
34. Varshney, R.; Bhadauria, S.; Gaur, M.S. A Review: Biological Synthesis of Silver and Copper Nanoparticles. *Nano Biomed. Eng.* **2012**, *4*, 99–106. [[CrossRef](#)]
35. Thiruvengadam, M.; Chung, I.M.; Gomathi, T.; Ansari, M.A.; Gopiesh Khanna, V.; Babu, V.; Rajakumar, G. Synthesis, characterization and pharmacological potential of green synthesized copper nanoparticles. *Bioprocess Biosyst. Eng.* **2019**, *42*, 1769–1777. [[CrossRef](#)]

36. Powar, N.S.; Patel, V.J.; Pagare, P.K.; Pandav, R.S. Cu Nanoparticle: Synthesis, Characterization and Application. *Chem. Methodol.* **2019**, *3*, 457–480. [\[CrossRef\]](#)
37. Guzman, A.; Arroyo, J.; Verde, L.; Rengifo, J. Synthesis and Characterization of Copper Nanoparticles/Polyvinyl Chloride (Cu NPs/PVC) Nanocomposites. *Procedia Mater. Sci.* **2015**, *9*, 298–304. [\[CrossRef\]](#)
38. Bhagat, M.; Anand, R.; Sharma, P.; Rajput, P.; Sharma, N.; Singh, K. Review—Multifunctional Copper Nanoparticles: Synthesis and Applications. *ECS J. Solid State Sci. Technol.* **2021**, *10*, 063011. [\[CrossRef\]](#)
39. Park, B.K.; Jeong, S.; Kim, D.; Moon, J.; Lim, S.; Kim, J.S. Synthesis and size control of monodisperse copper nanoparticles by polyol method. *J. Colloid Interface Sci.* **2007**, *311*, 417–424. [\[CrossRef\]](#)
40. Hikmah, N.; Idrus, N.F.; Jai, J.; Hadi, A. Synthesis and characterization of silver-copper core-shell nanoparticles using polyol method for antimicrobial agent. *IOP Conf. Ser. Earth Environ. Sci.* **2016**, *36*, 012050. [\[CrossRef\]](#)
41. Su, X.; Zhao, J.; Bala, H.; Zhu, Y.; Gao, Y.; Ma, S.; Wang, Z. Fast Synthesis of Stable Cubic Copper Nanocages in the Aqueous Phase. *J. Phys. Chem. C* **2007**, *111*, 14689–14693. [\[CrossRef\]](#)
42. Karaca, T.; Sevim, M.; Metin, Ö. Facile Synthesis of Monodisperse Copper–Platinum Alloy Nanoparticles and Their Superb Catalysis in the Hydrolytic Dehydrogenation of Ammonia Borane and Hydrazine Borane. *ChemCatChem* **2017**, *9*, 4185–4190. [\[CrossRef\]](#)
43. Wu, C.; Mosher, B.; Zeng, T. One-step green route to narrowly dispersed copper nanocrystals. *J. Nanoparticle Res.* **2006**, *8*, 965–969. [\[CrossRef\]](#)
44. Gyasi-Antwi, D.; Boansi, A.O.; Mensah, P.K. Impact resistance and electrical conductivity of copper nanoparticle-Milicia excels sawdust composites. *J. Appl. Sci. Technol.* **2019**, *23*, 46–50.
45. Gawande, M.B.; Goswami, A.; Felpin, F.X.; Asefa, T.; Huang, X.; Silva, R.; Zou, X.; Zboril, R.; Varma, R.S. Cu and Cu-Based Nanoparticles: Synthesis and Applications in Catalysis. *Chem. Rev.* **2016**, *116*, 3722–3811. [\[CrossRef\]](#) [\[PubMed\]](#)
46. Shenoy, U.; Shetty, N. A Simple Solution Phase Synthesis of Copper Nanofluid Using Single-step Glucose Reduction Method. *Synth. React. Inorg. Met. -Org. Nano-Met. Chem.* **2013**, *43*, 343–348. [\[CrossRef\]](#)
47. Wang, Y.; Duan, X.; Zheng, J.; Lin, H.; Yuan, Y.; Ariga, H.; Takakusagi, S.; Asakura, K. Remarkable enhancement of Cu catalyst activity in hydrogenation of dimethyl oxalate to ethylene glycol using gold. *Catal. Sci. Technol.* **2012**, *2*, 1637–1639. [\[CrossRef\]](#)
48. Katwal, R.; Kaur, H.; Sharma, G.; Naushad, M.; Pathania, D. Electrochemical synthesized copper oxide nanoparticles for enhanced photocatalytic and antimicrobial activity. *J. Ind. Eng. Chem.* **2015**, *31*, 173–184. [\[CrossRef\]](#)
49. Allocati, N.; Masulli, M.; Alexeyev, M.F.; Di Ilio, C. *Escherichia coli* in Europe: An Overview. *Int. J. Environ. Res. Public Health* **2013**, *10*, 6235–6254. [\[CrossRef\]](#)
50. Bastidas-Caldes, C.; de Waard, J.H.; Salgado, M.S.; Villacís, M.J.; Coral-Almeida, M.; Yamamoto, Y.; Calvopiña, M. Worldwide Prevalence of mcr-mediated Colistin-Resistance *Escherichia coli* in Isolates of Clinical Samples, Healthy Humans, and Livestock—A Systematic Review and Meta-Analysis. *Pathogens* **2022**, *11*, 659. [\[CrossRef\]](#)
51. Tong, S.Y.C.; Davis, J.S.; Eichenberger, E.; Holland, T.L.; Fowler, V.G. *Staphylococcus aureus* Infections: Epidemiology, Pathophysiology, Clinical Manifestations, and Management. *Clin. Microbiol. Rev.* **2015**, *28*, 603–661. [\[CrossRef\]](#)
52. Kumar, S.; Anwer, R.; Yadav, M.; Sehrawat, N.; Singh, M.; Kumar, V. Molecular Typing and Global Epidemiology of *Staphylococcus aureus*. *Curr. Pharmacol. Rep.* **2021**, *7*, 179–186. [\[CrossRef\]](#)
53. Rabiee, N.; Bagherzadeh, M.; Kiani, M.; Ghadiri, A.M.; Etesamifar, F.; Jaberizadeh, A.H.; Shakeri, A. Biosynthesis of Copper Oxide Nanoparticles with Potential Biomedical Applications. *Int. J. Nanomed.* **2020**, *15*, 3983–3999. [\[CrossRef\]](#) [\[PubMed\]](#)
54. Haider, M.K.; Ullah, A.; Sarwar, M.N.; Saito, Y.; Sun, L.; Park, S.; Kim, I.S. Lignin-mediated in-situ synthesis of CuO nanoparticles on cellulose nanofibers: A potential wound dressing material. *Int. J. Biol. Macromol.* **2021**, *173*, 315–326. [\[CrossRef\]](#) [\[PubMed\]](#)
55. Naz, S.; Gul, A.; Zia, M. Toxicity of copper oxide nanoparticles: A review study. *IET Nanobiotechnol.* **2020**, *14*, 1–13. [\[CrossRef\]](#) [\[PubMed\]](#)
56. Fakhar-e-Alam, M.; Shafiq, Z.; Mahmood, A.; Atif, M.; Anwar, H.; Hanif, A.; Yaqub, N.; Farooq, W.A.; Fatehmulla, A.; Ahmad, S.; et al. Assessment of green and chemically synthesized copper oxide nanoparticles against hepatocellular carcinoma. *J. King Saud Univ. Sci.* **2021**, *33*, 101669. [\[CrossRef\]](#)
57. Kalaiarasi, A.; Sankar, R.; Anusha, C.; Saravanan, K.; Aarthi, K.; Karthic, S.; Mathuram, T.L.; Ravikumar, V. Copper oxide nanoparticles induce anticancer activity in A549 lung cancer cells by inhibition of histone deacetylase. *Biotechnol. Lett.* **2018**, *40*, 249–256. [\[CrossRef\]](#)
58. Elsayed, A.M.; Sherif, N.M.; Hassan, N.S.; Althobaiti, F.; Hanafy, N.A.N.; Sahyon, H.A. Novel quercetin encapsulated chitosan functionalized copper oxide nanoparticles as anti-breast cancer agent via regulating p53 in rat model. *Int. J. Biol. Macromol.* **2021**, *185*, 134–152. [\[CrossRef\]](#)
59. Mahmood, R.I.; Kadhim, A.A.; Ibraheem, S.; Albukhaty, S.; Mohammed-Salih, H.S.; Abbas, R.H.; Jabir, M.S.; Mohammed, M.K.A.; Nayef, U.M.; AlMalki, F.A.; et al. Biosynthesis of copper oxide nanoparticles mediated *Annona muricata* as cytotoxic and apoptosis inducer factor in breast cancer cell lines. *Sci. Rep.* **2022**, *12*, 16165. [\[CrossRef\]](#)

60. Chen, H.; Feng, X.; Gao, L.; Mickymaray, S.; Paramasivam, A.; Abdulaziz Alfaiz, F.; Almasmoum, H.A.; Ghaith, M.M.; Almainani, R.A.; Aziz Ibrahim, I.A. Inhibiting the PI3K/AKT/mTOR signalling pathway with copper oxide nanoparticles from *Houttuynia cordata* plant: Attenuating the proliferation of cervical cancer cells. *Artif. Cells Nanomed. Biotechnol.* **2021**, *49*, 240–249. [\[CrossRef\]](#)
61. Benguigui, M.; Weitz, I.S.; Timaner, M.; Kan, T.; Shechter, D.; Perlman, O.; Sivan, S.; Raviv, Z.; Azhari, H.; Shaked, Y. Copper oxide nanoparticles inhibit pancreatic tumor growth primarily by targeting tumor initiating cells. *Sci. Rep.* **2019**, *9*, 12613. [\[CrossRef\]](#)
62. Li, C.; Li, Y.; Ding, C. The Role of Copper Homeostasis at the Host-Pathogen Axis: From Bacteria to Fungi. *Int. J. Mol. Sci.* **2019**, *20*, 175. [\[CrossRef\]](#)
63. Burkhead, J.L.; Gogolin Reynolds, K.A.; Abdel-Ghany, S.E.; Cohu, C.M.; Pilon, M. Copper homeostasis. *New Phytol.* **2009**, *182*, 799–816. [\[CrossRef\]](#) [\[PubMed\]](#)
64. Lutsenko, S.; Roy, S.; Tsvetkov, P. Mammalian copper homeostasis: Physiological roles and molecular mechanisms. *Physiol. Rev.* **2024**, *105*, 441–491. [\[CrossRef\]](#) [\[PubMed\]](#)
65. Festa, R.A.; Thiele, D.J. Copper: An essential metal in biology. *Curr. Biol.* **2011**, *21*, R877–R883. [\[CrossRef\]](#) [\[PubMed\]](#)
66. Ji, P.; Wang, P.; Chen, H.; Xu, Y.; Ge, J.; Tian, Z.; Yan, Z. Potential of Copper and Copper Compounds for Anticancer Applications. *Pharmaceuticals* **2023**, *16*, 234. [\[CrossRef\]](#)
67. Xu, S.; Liu, D.; Chang, T.; Wen, X.; Ma, S.; Sun, G.; Wang, L.; Chen, S.; Xu, Y.; Zhang, H. Cuproptosis-Associated lncRNA Establishes New Prognostic Profile and Predicts Immunotherapy Response in Clear Cell Renal Cell Carcinoma. *Front. Genet.* **2022**, *13*, 938259. [\[CrossRef\]](#)
68. Greish, K.; Pittalà, V.; Taurin, S.; Taha, S.; Bahman, F.; Mathur, A.; Jasim, A.; Mohammed, F.; El-Deeb, I.M.; Fredericks, S.; et al. Curcumin–Copper Complex Nanoparticles for the Management of Triple-Negative Breast Cancer. *Nanomaterials* **2018**, *8*, 884. [\[CrossRef\]](#)
69. Hu, Y.; Qian, Y.; Wei, J.; Jin, T.; Kong, X.; Cao, H.; Ding, K. The Disulfiram/Copper Complex Induces Autophagic Cell Death in Colorectal Cancer by Targeting ULK1. *Front. Pharmacol.* **2021**, *12*, 752825. [\[CrossRef\]](#)
70. Al-Zharani, M.; Qurtam, A.A.; Daoush, W.M.; Eisa, M.H.; Aljarba, N.H.; Alkahtani, S.; Nasr, F.A. Antitumor effect of copper nanoparticles on human breast and colon malignancies. *Environ. Sci. Pollut. Res.* **2021**, *28*, 1587–1595. [\[CrossRef\]](#)
71. Szewczyk, O.K.; Roszczenko, P.; Czarnomysy, R.; Bielawska, A.; Bielawski, K. An Overview of the Importance of Transition-Metal Nanoparticles in Cancer Research. *Int. J. Mol. Sci.* **2022**, *23*, 6688. [\[CrossRef\]](#)
72. Razmara, P.; Lari, E.; Mohaddes, E.; Zhang, Y.; Goss, G.G.; Pyle, G.G. The effect of copper nanoparticles on olfaction in rainbow trout (*Oncorhynchus mykiss*). *Environ. Sci. Nano* **2019**, *6*, 2094–2104. [\[CrossRef\]](#)
73. Razmara, P.; Sharpe, J.; Pyle, G.G. Rainbow trout (*Oncorhynchus mykiss*) chemosensory detection of and reactions to copper nanoparticles and copper ions. *Environ. Pollut.* **2020**, *260*, 113925. [\[CrossRef\]](#) [\[PubMed\]](#)
74. Al-Sagheer, L.A.M.; Elsayed, W.; Al-Ghamdi, A.A.; Alshehrie, A. Light interaction with the copper nanocrystals with various sizes prepared via portulaca oleracea assisted polyol technique. *Optik* **2020**, *203*, 163901. [\[CrossRef\]](#)
75. Pascu, B.; Negrea, A.; Ciopec, M.; Duteanu, N.; Negrea, P.; Bumm, L.A.; Grad, O.; Nemeş, N.S.; Mihalcea, C.; Duda-Seiman, D.M. Silver Nanoparticle Synthesis via Photochemical Reduction with Sodium Citrate. *Int. J. Mol. Sci.* **2023**, *24*, 255. [\[CrossRef\]](#) [\[PubMed\]](#)
76. Oliveira, J.; Prado, A.; Keijok, W.; Ribeiro, M.R.N.; Pontes, M.; Nogueira, B.; Guimarães, M. A helpful method for controlled synthesis of monodisperse gold nanoparticles through response surface modeling. *Arab. J. Chem.* **2017**, *13*, 216–226. [\[CrossRef\]](#)
77. Akintelu, S.A.; Oyebamiji, A.F.; Olugbelko, S.C.; Latona, D.F. Green chemistry approach towards the synthesis of copper nanoparticles and its potential applications as therapeutic agents and environmental control. *Curr. Res. Green Sustain. Chem.* **2021**, *4*, 100176. [\[CrossRef\]](#)
78. Vijayaraghavan, K.; Ashokkumar, T. Plant-mediated biosynthesis of metallic nanoparticles: A review of literature, factors affecting synthesis, characterization techniques and applications. *J. Environ. Chem. Eng.* **2017**, *5*, 4866–4883. [\[CrossRef\]](#)
79. Bali, R.; Harris, A.T. Biogenic Synthesis of Au Nanoparticles Using Vascular Plants. *Ind. Eng. Chem. Res.* **2010**, *49*, 12762–12772. [\[CrossRef\]](#)
80. Wu, H.; Zhang, H. Preparation of Novel Nanomaterial and Its Application in Food Industry. *Foods* **2022**, *11*, 1382. [\[CrossRef\]](#)
81. Lizama-Tzec, F.I.; Canché-Canul, L.; Oskam, G. Electrodeposition of copper into trenches from a citrate plating bath. *Electrochim. Acta* **2011**, *56*, 9391–9396. [\[CrossRef\]](#)
82. Rode, S.; Henninot, C.; Vallières, C.; Matlosz, M. Complexation Chemistry in Copper Plating from Citrate Baths. *J. Electrochem. Soc.* **2004**, *151*, C405. [\[CrossRef\]](#)
83. Daniele, P.G.; Ostacoli, G.; Zerbinati, O.; Sammartano, S.; De Robertis, A. Mixed metal complexes in solution. Thermodynamic and spectrophotometric study of copper(II)-citrate heterobinuclear complexes with nickel(II), zinc(II) or cadmium(II) in aqueous solution. *Transit. Met. Chem.* **1988**, *13*, 87–91. [\[CrossRef\]](#)
84. Glavee, G.N.; Klabunde, K.J.; Sorensen, C.M.; Hadjipanayis, G.C. Borohydride Reduction of Nickel and Copper Ions in Aqueous and Nonaqueous Media. Controllable Chemistry Leading to Nanoscale Metal and Metal Boride Particles. *Langmuir* **1994**, *10*, 4726–4730. [\[CrossRef\]](#)

85. Shahbazi, N.; Zare-Dorabei, R. A Facile Colorimetric and Spectrophotometric Method for Sensitive Determination of Metformin in Human Serum Based on Citrate-Capped Gold Nanoparticles: Central Composite Design Optimization. *ACS Omega* **2019**, *4*, 17519–17526. [\[CrossRef\]](#)
86. Wang, D.; Khan, W.U.; Tang, Z.; Wang, Y. Applicability Evaluation of Bright Green-Emitting Carbon Dots in the Solid State for White Light-Emitting Diodes. *Chem. Asian J.* **2018**, *13*, 292–298. [\[CrossRef\]](#) [\[PubMed\]](#)
87. Alhumaimess, M.S.; Essawy, A.A.; Kamel, M.M.; Alsohaimi, I.H.; Hassan, H.M. Biogenic-Mediated Synthesis of Mesoporous Cu₂O/CuO Nano-Architectures of Superior Catalytic Reductive towards Nitroaromatics. *Nanomaterials* **2020**, *10*, 781. [\[CrossRef\]](#)
88. He, J.; Jiang, Y.; Peng, J.; Li, C.; Yan, B.; Wang, X. Fast synthesis of hierarchical cuprous oxide for nonenzymatic glucose biosensors with enhanced sensitivity. *J. Mater. Sci.* **2016**, *51*, 9696–9704. [\[CrossRef\]](#)
89. Yevdokymenko, V.Y.; Dobrozhan, O.; Pshenychnyi, R.; Opanasyuk, A.; Gnatenko, Y.; Bukivskii, A.; Bukivskij, P.; Gamernyk, R.; Klymov, O.; Muñoz-Sanjósé, V.; et al. The effect of annealing treatment on the structural and optical properties of nanostructured Cu_xO films obtained by 3D printing. *Mater. Sci. Semicond. Process.* **2023**, *161*, 107472. [\[CrossRef\]](#)
90. Beltrán-Partida, E.; Valdez Salas, B.N.; Valdez-Salas, E.; Pérez-Cortéz, G.; Nedev, N. Synthesis, Characterization, and In Situ Antifungal and Cytotoxicity Evaluation of Ascorbic Acid-Capped Copper Nanoparticles. *J. Nanomater.* **2019**, *2019*, 5287632. [\[CrossRef\]](#)
91. Rawat, R.; Tiwari, A.; Singh, M.K.; Mandal, R.K.; Pathak, A.P.; Tripathi, A. Effects on surface-enhanced Raman scattering from copper nanoparticles synthesized by laser ablation. *Radiat. Eff. Defects Solids* **2020**, *175*, 332–341. [\[CrossRef\]](#)
92. Sayson, L.V.A.; Lopez, J.M.; Estacio, E.S.; Salvador, A.A.; Somintac, A.S. Nanostructured CuO thin film deposited on stainless steel using spray pyrolysis as supercapacitor electrode. *Mater. Res. Express* **2019**, *6*, 125551. [\[CrossRef\]](#)
93. Pandoli, O.G.; Neto, R.J.G.; Oliveira, N.R.; Fingolo, A.C.; Corrêa, C.C.; Ghavami, K.; Strauss, M.; Santhiago, M. Ultra-highly conductive hollow channels guided by a bamboo bio-template for electric and electrochemical devices. *J. Mater. Chem. A* **2020**, *8*, 4030–4039. [\[CrossRef\]](#)
94. Prabhu, Y.; Rao, K.; Sai, V.; Tambur, P. A Facile biosynthesis of Copper nanoparticles: A micro-structural and antibacterial activity investigation. *J. Saudi Chem. Soc.* **2017**, *21*, 180–185. [\[CrossRef\]](#)
95. Singh, A.; Raykar, V. Microwave synthesis of silver nanofluids with polyvinylpyrrolidone (PVP) and their transport properties. *Colloid Polym. Sci.* **2008**, *286*, 1667–1673. [\[CrossRef\]](#)
96. Marinello, F.; Carmignato, S.; Voltan, A.; Savio, E.; De Chiffre, L. Error Sources in Atomic Force Microscopy for Dimensional Measurements: Taxonomy and Modeling. *J. Manuf. Sci. Eng.* **2010**, *132*, 0309031–0309038. [\[CrossRef\]](#)
97. Von White, G., II; Kersch, P.; Brown, R.M.; Morella, J.D.; McAllister, W.; Dean, D.; Kitchens, C.L. Green Synthesis of Robust, Biocompatible Silver Nanoparticles Using Garlic Extract. *J. Nanomater.* **2012**, *2012*, 730746. [\[CrossRef\]](#) [\[PubMed\]](#)
98. Lewis, J.S., II; PharmD; FIDSA. *Performance Standards for Antimicrobial Susceptibility Testing*, 34th ed.; Clinical and Laboratory Standards Institute: Wayne, PA, USA, 2020; Available online: <https://clsi.org/standards/products/microbiology/documents/m100/> (accessed on 12 December 2024).
99. Brook, I.; Frazier, E.H. Aerobic and anaerobic microbiology of infection after trauma. *Am. J. Emerg. Med.* **1998**, *16*, 585–591. [\[CrossRef\]](#) [\[PubMed\]](#)
100. Delgado, A.; Guddati, A.K. Infections in Hospitalized Cancer Patients. *World J. Oncol.* **2021**, *12*, 195–205. [\[CrossRef\]](#)
101. Pascu, B.; Negrea, A.; Ciopec, M.; Duteanu, N.; Negrea, P.; Nemeş, N.S.; Seiman, C.; Marian, E.; Micle, O. A Green, Simple and Facile Way to Synthesize Silver Nanoparticles Using Soluble Starch. pH Studies and Antimicrobial Applications. *Materials* **2021**, *14*, 4765. [\[CrossRef\]](#)
102. Yakoup, A.Y.; Kamel, A.G.; Elbermawy, Y.; Abdelsattar, A.S.; El-Shibiny, A. Characterization, antibacterial, and cytotoxic activities of silver nanoparticles using the whole biofilm layer as a macromolecule in biosynthesis. *Sci. Rep.* **2024**, *14*, 364. [\[CrossRef\]](#)
103. Selvarani, M. Investigation of the synergistic antibacterial action of copper nanoparticles on certain antibiotics against human pathogens. *Int. J. Pharm. Pharm. Sci.* **2018**, *10*, 83–86.
104. Fu, Y.; Chang, F.M.J.; Giedroc, D.P. Copper Transport and Trafficking at the Host–Bacterial Pathogen Interface. *Acc. Chem. Res.* **2014**, *47*, 3605–3613. [\[CrossRef\]](#) [\[PubMed\]](#)
105. Moloney, J.N.; Cotter, T.G. ROS signalling in the biology of cancer. *Semin. Cell Dev. Biol.* **2018**, *80*, 50–64. [\[CrossRef\]](#) [\[PubMed\]](#)
106. Ma, X.; Zhou, S.; Xu, X.; Du, Q. Copper-containing nanoparticles: Mechanism of antimicrobial effect and application in dentistry—a narrative review. *Front. Surg.* **2022**, *9*, 905892. [\[CrossRef\]](#)
107. Gunther, M.R.; Hanna, P.M.; Mason, R.P.; Cohen, M.S. Hydroxyl radical formation from cuprous ion and hydrogen peroxide: A spin-trapping study. *Arch. Biochem. Biophys.* **1995**, *316*, 515–522. [\[CrossRef\]](#)
108. Cheloni, G.; Marti, E.; Slaveykova, V.I. Interactive effects of copper oxide nanoparticles and light to green alga *Chlamydomonas reinhardtii*. *Aquat. Toxicol.* **2016**, *170*, 120–128. [\[CrossRef\]](#)
109. Bhat, S.; Muthunatarajan, S.; Mulki, S.S.; Archana Bhat, K.; Kotian, K.H. Bacterial Infection among Cancer Patients: Analysis of Isolates and Antibiotic Sensitivity Pattern. *Int. J. Microbiol.* **2021**, *2021*, 8883700. [\[CrossRef\]](#)

110. Abdollahzadeh, H.; Pazhang, Y.; Zamani, A.; Sharafi, Y. Green synthesis of copper oxide nanoparticles using walnut shell and their size dependent anticancer effects on breast and colorectal cancer cell lines. *Sci. Rep.* **2024**, *14*, 20323. [[CrossRef](#)]
111. Franke, R.; Hinkelmann, B.; Fetz, V.; Stradal, T.; Sasse, F.; Klawonn, F.; Brönstrup, M. xCELLanalyzer: A Framework for the Analysis of Cellular Impedance Measurements for Mode of Action Discovery. *SLAS Discov.* **2019**, *24*, 213–223. [[CrossRef](#)]
112. Atienzar, F.A.; Gerets, H.; Tilmant, K.; Toussaint, G.; Dhalluin, S. Evaluation of impedance-based label-free technology as a tool for pharmacology and toxicology investigations. *Biosensors* **2013**, *3*, 132–156. [[CrossRef](#)]

Disclaimer/Publisher’s Note: The statements, opinions and data contained in all publications are solely those of the individual author(s) and contributor(s) and not of MDPI and/or the editor(s). MDPI and/or the editor(s) disclaim responsibility for any injury to people or property resulting from any ideas, methods, instructions or products referred to in the content.